

ORIGINAL RESEARCH

 OPEN ACCESS

G-CSF regulates macrophage phenotype and associates with poor overall survival in human triple-negative breast cancer

Maija Hollmén^a, Sinem Karaman^a, Simon Schwager^a, Angela Lisibach^a, Ailsa J. Christiansen^a, Mikael Maksimow^b, Zsuzsanna Varga^c, Sirpa Jalkanen^b, and Michael Detmar^a

^aInstitute of Pharmaceutical Sciences, Swiss Federal Institute of Technology, ETH Zürich, Zurich, Switzerland; ^bMedicity Research Laboratory, University of Turku, Turku, Finland; ^cInstitute of Surgical Pathology, University Hospital Zürich, Zurich, Switzerland

ABSTRACT

Tumor-associated macrophages (TAMs) have been implicated in the promotion of breast cancer growth and metastasis, and a strong infiltration by TAMs has been associated with estrogen receptor (ER)-negative tumors and poor prognosis. However, the molecular mechanisms behind these observations are unclear. We investigated macrophage activation in response to co-culture with several breast cancer cell lines (T47D, MCF-7, BT-474, SKBR-3, Cal-51 and MDA-MB-231) and found that high granulocyte colony-stimulating factor (G-CSF) secretion by the triple-negative breast cancer (TNBC) cell line MDA-MB-231 gave rise to immunosuppressive HLA-DR^{lo} macrophages that promoted migration of breast cancer cells via secretion of TGF- α . In human breast cancer samples ($n = 548$), G-CSF was highly expressed in TNBC ($p < 0.001$) and associated with CD163⁺ macrophages ($p < 0.0001$), poorer overall survival (OS) ($p = 0.021$) and significantly increased numbers of TGF- α ⁺ cells. While G-CSF blockade in the 4T1 mammary tumor model promoted maturation of MHCII^{hi} blood monocytes and TAMs and significantly reduced lung metastasis, anti-CSF-1R treatment promoted MHCII^{lo}F4/80^{hi}MR^{hi} anti-inflammatory TAMs and enhanced lung metastasis in the presence of high G-CSF levels. Combined anti-G-CSF and anti-CSF-1R therapy significantly increased lymph node metastases, possibly via depletion of the so-called “gate-keeper” subcapsular sinus macrophages. These results indicate that G-CSF promotes the anti-inflammatory phenotype of tumor-induced macrophages when CSF-1R is inhibited and therefore caution against the use of M-CSF/CSF-1R targeting agents in tumors with high G-CSF expression.

Abbreviations: CD163, Hemoglobin/haptoglobin scavenger receptor; CD169, Sialoadhesin, Siglec-1; CM, Conditioned media; CSF-1R, Colony-stimulating factor 1 receptor; EGFR, Epidermal growth factor receptor; ER, Estrogen receptor; G-CSF, Granulocyte colony-stimulation factor; G-CSFR, Granulocyte colony-stimulating factor receptor; gMFI, geometric mean fluorescence intensity; HER2, Epidermal growth factor receptor 2; IFN γ , Interferon gamma; LN, Lymph node; LPS, Lipopolysaccharide; M1, Classically activated macrophage; M2, Alternatively activated macrophage; M-CSF, Macrophage colony-stimulating factor; MR, Macrophage mannose receptor; OS, Overall survival; PgR, Progesterone receptor; TGF- α , Transforming growth factor α ; TNBC, Triple-negative breast cancer; TAM, Tumor-associated macrophage; TMA, Tumor micro-array

ARTICLE HISTORY

Received 12 June 2015
Revised 14 October 2015
Accepted 27 October 2015

KEYWORDS


CSF3; HLA-DR; M-CSF; TGF- α ; TNBC; tumor-associated macrophages

Introduction

Breast cancer is one of the leading causes of death in women worldwide.¹ Although improvement in both early breast cancer detection and treatment options has reduced breast cancer mortality, not all patients have benefited from these advances. TNBC is a definition of breast tumors that do not express the ER or the progesterone receptor (PgR), and do not have an amplification or overexpression of the epidermal growth factor receptor 2 gene (HER2) and thus cannot be treated with anti-hormonal therapy or anti-HER2 agents. TNBC represents 10–20% of invasive breast cancers and has been associated with African-American race, younger age, *BRCA1* mutations and poorer prognosis.² Its heterogeneity and the uncharacterized molecular pathways underlying the pathology of TNBC have made this breast cancer subtype extremely challenging to treat and manage.³

The development of breast cancers, such as TNBC largely depends on the contribution of stromal cells in providing growth and metastasis supporting signals as well as aiding immune escape from the host.⁴ These tumor-supporting actions are vastly mediated by TAMs that are abundantly present in the leukocyte infiltrate of breast cancers with poor prognosis⁵ and ER- negative subtype.⁶ In contrast to the IFN γ and lipopolysaccharide (LPS)-driven classically activated (M1) macrophages with high microbicidal activity, immuno-stimulatory functions and tumor cytotoxicity, TAMs resemble the alternatively activated (M2) macrophages, which promote tissue repair, angiogenesis, and favor tumor progression.⁷ The polarization toward this “tolerogenic” phenotype is mainly mediated by the anti-inflammatory cytokines IL-4 and IL-13.⁸ In response, the M2 polarized macrophages upregulate several

CONTACT Michael Detmar  michael.detmar@pharma.ethz.ch

 Supplemental data for this article can be accessed on the publisher's website.

Published with license by Taylor & Francis Group, LLC © Maija Hollmén, Sinem Karaman, Simon Schwager, Angela Lisibach, Ailsa J. Christiansen, Mikael Maksimow, Zsuzsanna Varga, Sirpa Jalkanen, and Michael Detmar

This is an Open Access article distributed under the terms of the Creative Commons Attribution-Non-Commercial License (<http://creativecommons.org/licenses/by-nc/3.0/>), which permits unrestricted non-commercial use, distribution, and reproduction in any medium, provided the original work is properly cited. The moral rights of the named author(s) have been asserted.

phenotypic markers such as macrophage mannose receptor (MR; CD206/*MRC1*)⁹ and hemoglobin/haptoglobin scavenger receptor CD163,¹⁰ and secrete high levels of IL-10.¹¹

Several attempts have been made to inhibit macrophage activation in cancer. Macrophage colony-stimulating factor (M-CSF, CSF-1) is a major contributor of TAM infiltration and increased tumor growth.^{12,13} Efforts in blocking the M-CSF/CSF-1R signaling pathway have been reported to reduce tumor growth in breast cancer xenograft models.^{14,15} This, along with other observations of the beneficial effect of targeting CSF-1R in various cancers,¹⁶⁻¹⁸ has led to the initiation of phase I clinical trials with either a monoclonal antibody targeting CSF-1R (IMC-CS4) or a small molecule inhibitor of CSF-1R (PLX3397) alone or in combination with chemotherapy to treat solid tumors (www.clinicaltrials.gov).

G-CSF is a cytokine that stimulates the survival, proliferation, differentiation and function of neutrophil precursors and mature neutrophils via its receptor G-CSFR. It also mobilizes hematopoietic stem cells from the bone marrow and has been utilized for this action in hematopoietic stem cell transplantation and in the treatment of chemotherapy-induced febrile neutropenia. G-CSF has also been reported to modulate inflammatory responses since mice pretreated with G-CSF were protected against an otherwise lethal dose of LPS.¹⁹ The immune modulatory functions of G-CSF may also potentially be mediated by monocyte activation since G-CSF mobilized monocytes carry surface bound IL-10²⁰ and inhibit the release of IL-12 and tumor necrosis factor (TNF)- α after LPS stimulation.²¹

In the present study, we found that G-CSF, similar to M-CSF, can modulate monocyte differentiation into anti-inflammatory macrophages that have tumor-supporting functions. Importantly, we observed that human breast cancer patients with high G-CSF expression have a significantly poorer prognosis than low G-CSF expressing patients in TNBC and that this was associated with higher numbers of CD163⁺ macrophages. In the 4T1 mouse mammary tumor model, the inhibition of CSF-1R signaling led to increased lung metastasis and an abundance of MHCII^{lo} anti-inflammatory monocytes and TAMs when G-CSF was present. However, when G-CSF was also blocked, the incidence of LN metastases was dramatically increased, probably due to the anti-CSF-1R mediated depletion of subcapsular sinus macrophages.

Results

Alternative activation of human CD14⁺ monocytes/macrophages by MDA-MB-231 cells

To mimic the interplay between tumor-infiltrating monocytes and cancer cells, we cultured three human breast cancer cell lines, representing human ER⁺ (T47D), HER2⁺ (SKBR-3) or triple-negative (MDA-MB-231) breast cancer, in a transwell co-culture system with freshly isolated human CD14⁺ peripheral blood monocytes. In general, the single cultured monocytes in RPMI demonstrated a pro-inflammatory phenotype when activated by adhesion to the polyester (PET) membrane (Fig. S1A). Under co-culture, the MDA-MB-231-activated monocytes upregulated MR (intracellular) and demonstrated

elongated cell morphology compared to monocytes co-cultured with either T47D or SKBR-3 cells (Fig. 1A). Quantification of MR expression showed a significant increase in MR⁺/CD68⁺ cells within the MDA-MB-231 co-culture as compared to the other stimuli (Fig. 1A; day two $p = 0.0017$, day 5 $p < 0.0001$). Functionally, the MDA-MB-231 educated macrophages developed impaired antigen processing over the incubation time as only 15% of cells were able to process fluorescently labeled ovalbumin at day 5 compared to 100% at day 2 (Fig. 1B; $p = 0.0001$).

To exclude the effect of adhesion in activating macrophage polarization, the monocytes were cultured in ultra-low attachment plates in different cancer cell conditioned media collected from three ER-positive cell lines (T47D, MCF-7 and BT-474) and two TNBC lines (Cal-51 and MDA-MB-231). Flow cytometric analysis of cell surface MR expression together with HLA-DR expression demonstrated again that only MDA-MB-231 cells skewed the balance of MR (M2-marker) and HLA-DR (M1-marker) expression into an anti-inflammatory phenotype (Figs. 1C–E). The polarization difference resulted mainly from the downregulation of HLA-DR on MDA-MB-231 differentiated macrophages rather than by an upregulation of MR expression, at least at the cell surface level (Fig. 1E; percentage of CD14⁺ cell positive for HLA-DR $p = 0.0006$ and MR $p = 0.231$). Because of the high inter-individual variation in the geometric mean fluorescence intensities (gMFIs) of HLA-DR and MR expression, the levels of HLA-DR and MR on T47D differentiated macrophages were considered as baseline and used for normalization of the data. The individual gMFIs are shown in Fig. S1B.

G-CSF promotes differentiation of immunosuppressive HLA-DR^{lo} macrophages

To understand why MDA-MB-231 cells promoted HLA-DR^{lo} macrophages in contrast to the other cell lines, we screened 48 cytokines, chemokines and growth factors in MDA-MB-231 CM and compared the secretion profiles to the ones from T47D and SKBR-3 cells. While MDA-MB-231 cells showed high production of G-CSF (5,586 pg/mL), IL-8 (2,425 pg/mL) and VEGF (1,878 pg/mL), T47D cells produced high levels of stromal cell-derived factor-1 (SDF-1a/CXCL12; 2,173 pg/mL) (Fig. 2A). Because peripheral blood harvested from G-CSF-stimulated donors has been reported to contain a skewed Th2 CD4⁺ phenotype and a predominance of type 2 dendritic cells,²² we investigated whether G-CSF was responsible for the differential activation of co-cultured macrophages by MDA-MB-231 cells. The G-CSF treated macrophages increased MR expression and exhibited an elongated cell morphology (Fig. 2B). After eight days, 99% of CD68⁺ cells were also MR⁺ (Fig. 2B; $p < 0.0001$). Addition of a G-CSF-neutralizing antibody (α G-CSF) to MDA-MB-231 CM decreased the amount of MR⁺/CD68⁺ cells from 83% to 28% ($p = 0.0046$) after 8 d (Fig. 2B). Again, on the cell surface, MR expression did not dramatically change but HLA-DR expression was down regulated on monocytes/macrophages after a 4-d treatment with G-CSF compared to 1% AB serum-treated monocytes (Fig. 2C; $p = 0.032$). The G-CSF-differentiated monocytes

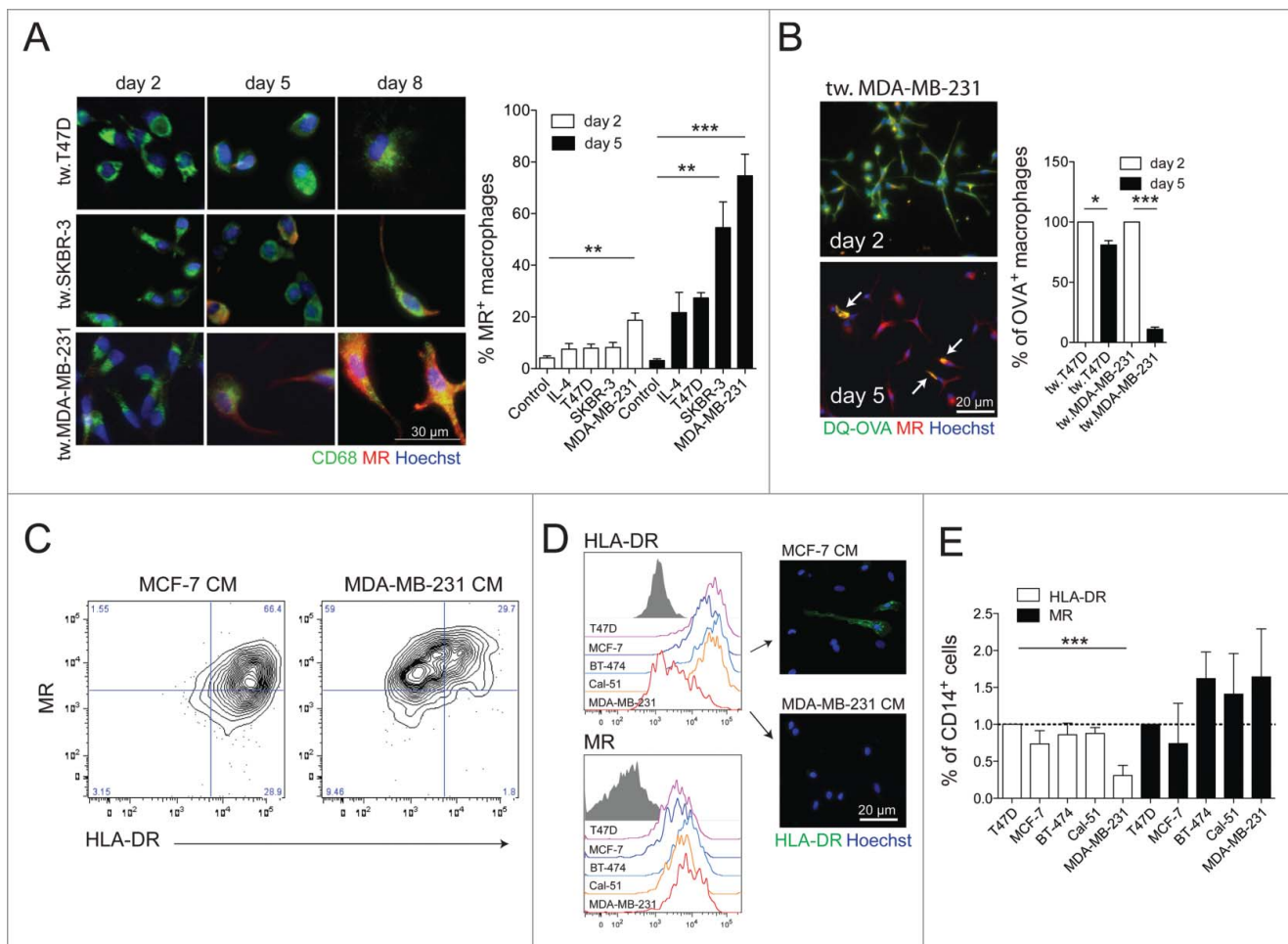


Figure 1. MDA-MB-231 cells alternatively activate human CD14⁺ monocytes. (A) Freshly isolated human CD14⁺ monocytes were cultured with three different breast cancer cell lines T47D (ER+), SKBR-3 (HER2+) and MDA-MB-231 (TN) in a transwell (tw.) co-culture system (ratio 1:1) and analyzed for changes in macrophage mannose receptor expression (MR) at indicated time points by immunofluorescence staining using anti-CD206 antibody (MR, red) and quantified as percentage of MR⁺ cells within the total number of CD68⁺ cells (green). Data were obtained from experiments performed in triplicates using four different monocyte donors and analyzed using one-way ANOVA with Tukey's multiple comparison test. Control wells (without cancer cells) contained RPMI alone (negative control) or 20 ng/mL IL-4 (positive control). (B) Monocytes from the experiment in (A) were incubated with DQ-ovalbumin for 2 h prior to fixation at indicated time points and the signal from processed ovalbumin-BODIPY (green) was quantified as percentage of green cells to the number of Hoechst positive nuclei and analyzed using two-tailed Student's t-test ($n = 3$, data combined from three independent experiments with triplicate wells each). The arrows in the lower panel point to the processed ovalbumin signal indicated by BODIPY fluorescence, which was significantly decreased at day 5 compared to day 2 for monocytes cultured with MDA-MB-231 cells. Representative plots (C) and histograms (D) of flow cytometric analyses of cell surface HLA-DR and MR expression on CD14⁺ monocytes cultured in CM collected from three estrogen receptor positive cell lines (T47D, MCF-7 and BT-474) and two TNBC lines (Cal-51 and MDA-MB-231). The monocytes were cultured (6 d) in ultra-low attachment plates to exclude the effect of adhesion on the expression levels of HLA-DR and MR. The gray-filled histogram represents the isotype control. Microscopic images of HLA-DR staining are shown on the right for MCF-7 and MDA-MB-231 CM cultured monocytes that were let to adhere overnight on culture slides. (E) Graphs from the flow cytometric analysis (in D) showing the % of CD14⁺ cells positive for HLA-DR and MR. The expression of HLA-DR and MR on T47D cultured monocytes were selected as baseline to control for inter-individual variation. Statistical significance was analyzed using one-way ANOVA with Tukey's multiple comparison test ($n = 3$).

suppressed CD4⁺ T-cell activation in response to tetanus toxoid, which was seen as a decrease in proliferation (Fig. 2D; $p = 0.019$) and lower IFN γ production (Fig. 2E) of CD4⁺ T-cells compared to CD4⁺ T-cells co-cultured with control monocytes.

G-CSF differentiated macrophages promote cancer cell migration via secretion of TGF- α

We have previously shown that MDA-MB-231-educated macrophages support tumor growth and have an anti-inflammatory phenotype.²³ To test whether G-CSF was also responsible for mediating tumor-supporting macrophages in MDA-MB-231 CM, we studied cancer cell migration toward control (1% AB), T47D CM, MDA-MB-231 CM and G-CSF

differentiated macrophages in a co-culture setting where the differentiated macrophages served as a source of chemotactic factors for the migrating cells. G-CSF polarized macrophages did not change migration of T47D cells compared to control macrophages, but the migration was significantly increased toward T47D CM activated macrophages (Fig. 3A; $p < 0.0001$). G-CSF differentiated macrophages, on the other hand, promoted the migration of MDA-MB-231 cells significantly more than 1% human serum or T47D CM differentiated macrophages (Fig. 3A; $p = 0.0076$). This suggested that G-CSF induced the macrophages to secrete a factor that was chemotactic for MDA-MB-231 cells, but not for T47D cells. We have previously reported that macrophages upregulate transforming growth factor- α (TGF- α) and oncostatin M (OSM) transcripts in co-culture with MDA-MB-231 cells.²³

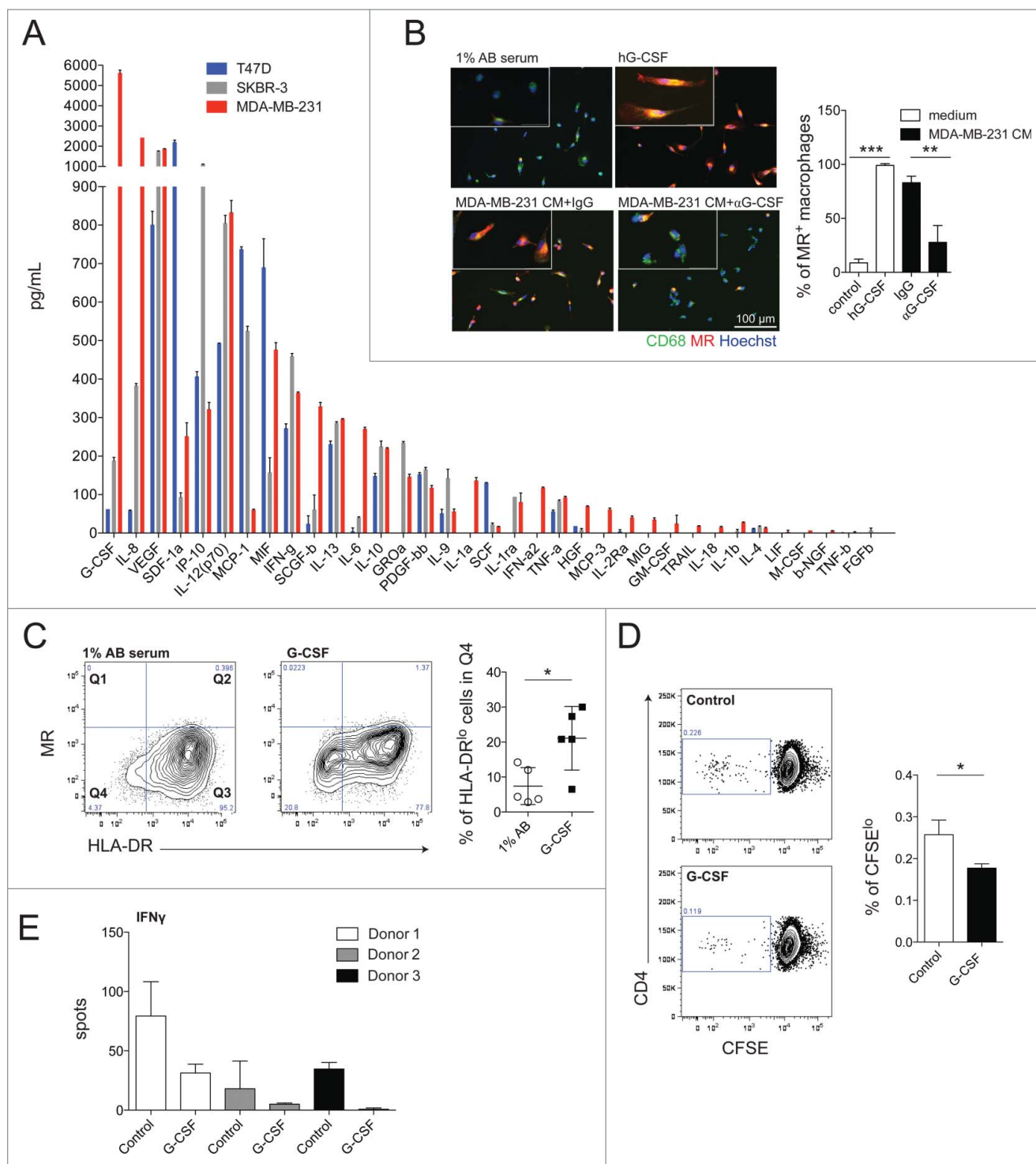


Figure 2. G-CSF is highly secreted by MDA-MB-231 cells and promotes differentiation of immunosuppressive HLA-DR low monocytes. (A) Cytokine, chemokine and growth factor secretion analysis of CM of single cultured T47D, SKBR-3 and MDA-MB-231 cells using Bio-plex pro assay Human Cytokine 21-plex and Human Cytokine 27-plex. Error bars represent intra-assay variation between duplicate samples. (B) Immunofluorescence images of human CD14⁺ monocytes cultured for 8 d in RPMI supplemented with either 1% human serum (AB) or 50 ng/mL recombinant human G-CSF (upper panel), MDA-MB-231 CM with 1 μ g/mL of IgG control or anti-G-CSF (lower panel). MR expression was analyzed using anti-CD206 antibody (MR, red) and quantified as percentage of MR⁺ cells within the total number of CD68⁺ cells (green). Statistical analysis was done using two-tailed Student's t-test ($n = 9$, data combined from three independent experiments with triplicate wells). (C) Representative plots of flow cytometric analyses of cell surface HLA-DR and MR expression on CD14⁺ monocytes cultured for 4 d (ultra-low attachment) in RPMI supplemented with 1% human serum (AB) or 50 ng/mL recombinant human G-CSF. The histogram shows the percent of CD14⁺ cells that expressed lower levels of HLA-DR (Q4), $n = 5$; Mann Whitney test. (D) CFSE-labeled CD4⁺ T cells from tetanus-toxoid-vaccinated healthy donors were incubated for 3 d with donor-matched CD14⁺ monocytes. The monocytes were collected 4 d prior T-cell co-culture to differentiate the cells with 1% human serum (AB) or 50 ng/mL recombinant human G-CSF as in C and pulsed with tetanus toxoid for 3 h before addition of T cells. T-cell proliferation was analyzed as the percent of cells appearing in the low CFSE gate by flow cytometry, $n = 4$, mean from triplicate wells; two-tailed Student's t-test. (E) ELISpot assay of IFN γ production of CD4⁺ T-cells in response to tetanus toxoid in the presence of control (1% AB) or G-CSF (50 ng/mL) differentiated monocytes as in (D), $n = 3$, mean from triplicate wells.

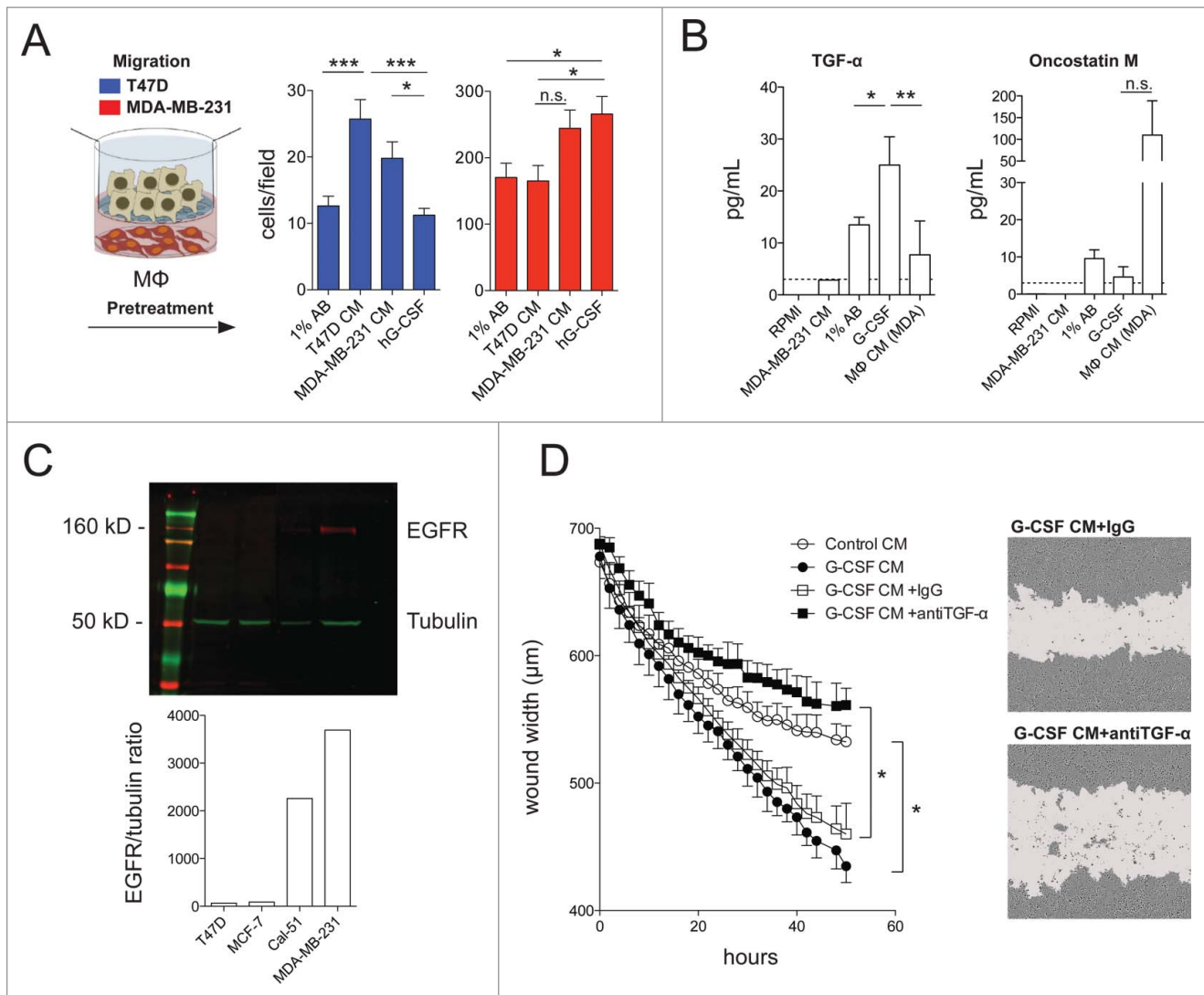


Figure 3. G-CSF-differentiated macrophages secrete TGF- α and selectively promote migration of EGFR expressing cells. (A) Freshly isolated CD14⁺ monocytes were pre-treated with 1% AB serum, T47D CM, MDA-MB-231 CM or 40 ng/mL hG-CSF in RPMI for 48 h. The pre-incubation media was washed and replaced with RPMI only and conditioned for 24 h. At this point, the cancer cells were placed on the collagen coated upper chamber and cancer cell migration toward the pretreated monocytes was analyzed after 6 h by counting the nuclei of transmigrated cells. The graphs represent the average number of transigrated nuclei per 10x microscope field from three independent experiments done in triplicates and was analyzed using one-way ANOVA with Tukey's multiple comparison test. (B) ELISA analysis of TGF- α and Oncostatin M levels measured from monocyte pre-treatment CM (n = 3) from the experiment shown in (A). Basal level of TGF- α and Oncostatin M in MDA-MB-231 CM is shown on graphs labeled MDA-MB-231 CM. M Φ CM (MDA) stands for CM from monocytes collected 24 h after a 48 h pre-treatment with MDA-MB-231 CM. Statistical analysis was done using one-way ANOVA with Tukey's multiple comparison test. (C) Western blot analysis of EGFR expression on T47D, MCF-7, Cal-51 and MDA-MB-231 cells. EGFR signal intensity was quantified against tubulin expression in each sample and represented in the graph as arbitrary fluorescence units. (D) Scratch wound migration of Cal-51 cells monitored every 2 h for a total of 48 h using the Incucyte ZOOM system. The Cal-51 cells were cultured in CM collected from monocytes grown in control medium or G-CSF as in Fig. 2C. The G-CSF-activated monocyte CM was supplemented with 5 μ g/mL of anti-TGF α or isotype control antibody before experimentation. Representative data from three independent experiments performed using CM from one monocyte donor where statistical significance was analyzed using two-way ANOVA.

TGF- α has been reported to drive triple-negative tumor invasion,²⁴ whereas OSM promotes EMT and a stem cell-like phenotype in breast cancer²⁵; both factors contribute to tumor aggressiveness. ELISA analysis of G-CSF-treated macrophage CM at day 2 indicated that G-CSF significantly increased the secretion of TGF- α compared to 1% AB serum or MDA-MB-231 CM-differentiated macrophages (Fig. 3B; $p = 0.0037$) but had no effect on OSM levels (Fig. 3B). The analysis of epidermal growth factor receptor (EGFR, receptor for TGF- α) expression on T47D, MCF-7 (both ER⁺), Cal-51, and MDA-MB-231 (both TNBC) cells revealed that only the TNBC cell lines expressed detectable amounts of EGFR (Fig. 3C) explaining why only MDA-MB-231 cells increased

migration toward macrophages in the presence of TGF- α . Since the oncogenic activity of MDA-MB-231 cells is driven by a KRAS mutation, we analyzed the feedback loop of G-CSF/TGF- α using the EGFR expressing Cal-51 TNBC cell line. In a scratch wound-healing assay, CM from G-CSF differentiated macrophages induced Cal-51 migration (wound closure) significantly more than control CM (Fig. 3D; $p = 0.028$). Blockade of TGF- α in the G-CSF CM significantly decreased migration of Cal-51 cells compared to IgG CM (Fig. 3D; $p = 0.03$). Addition of anti-TGF- α to normal growth medium with or without 10% FCS did not affect Cal-51 migration, indicating that the Cal-51 cells do not secrete TGF- α in an autocrine manner (data not shown).

High G-CSF expression in human breast cancer is significantly associated with TNBC and poorer overall survival

To investigate whether G-CSF was also present in the aggressive types of human breast cancer, we stained paraffin-embedded whole tumor sections (Table S1; ER⁺ n = 42; ER⁻ n = 10) with an antibody against G-CSF to analyze the level and location of this growth factor in large tumor areas. Because G-CSF staining of the tumor sections was very heterogeneous and mainly located at the invasive front of the tumors, the scoring of G-CSF staining intensity was done in the invasive areas. Four scores were assigned (0, 1, 2, and 3) where 0 represented negative and 3 high expression of G-CSF, as stated in detail in the Methods section and illustrated in Fig. S2A. For statistical analyses, the staining was classified as low (score 0/1) or high (score 2/3) (Fig. 4A). Of note, the adjacent normal mammary gland demonstrated high G-CSF staining of score 2 and was used as a positive control to assess staining quality. High G-CSF expression in the whole sections was significantly associated with the ER-negative subtype (Fig. S2B; $p = 0.02$) and grade 3 tumors (Fig. S2C; $p = 0.0059$).

In a larger set of human breast cancer samples (n = 548), including two tissue microarrays (Table 1; TMA21 and TMA174), we detected higher G-CSF expression in the triple-negative tumors compared to cancers expressing either ER⁺ or HER2⁺ or both. (Fig. 4B; $p < 0.001$ 0/1 vs. 2/3). High G-CSF expression in the TNBC patients was significantly correlated with poorer OS when compared to patients with low G-CSF expression (Fig. 4C; $p = 0.021$). We found an approximately 13 mo improvement in the median survival between high and low G-CSF expressing patients at 50% survival. Because G-CSF levels did not significantly correlate with tumor size ($p = 0.56$), grade ($p = 0.53$) or lymph node status ($p = 0.8$, Spearman's rho), a correction for these factors was not done for the G-CSF survival analysis.

Table 1. Clinicopathological parameters of breast cancer samples on tissue microarrays with mixed breast carcinomas (n = 641) and hormone receptor (ER/PgR) negative (n = 91) carcinomas.

		TMA mixed n = 641	TMA TN n = 91
Subtype	Ductal	474 (74%)	78 (86%)
	Lobular	79 (12%)	3 (3%)
	Other	62 (10%)	0
	Missing	26 (4%)	—
Hormone receptor status	ER positive	473 (74%)	0
	ER negative	103 (16%)	91 (100%)
	Missing	65 (9%)	—
HER2 status	HER2 positive	90 (14%)	8 (9%)
	HER2 negative	516 (80%)	83 (91%)
	Missing	35 (6%)	—
Grade	1	101 (16%)	0
	2	302 (47%)	5 (6%)
	3	206 (32%)	86 (94%)
	Missing	32 (5%)	—
Axillary nodal status	Positive	336 (52%)	48 (53%)
	Negative	211 (33%)	42 (46%)
	Missing	94 (15%)	1 (1%)
Stadium	pT1	266 (41%)	38 (42%)
	pT2	267 (42%)	44 (48%)
	pT3	48 (8%)	7 (8%)
	pT4	33 (5%)	2 (2%)
	Missing	27 (4%)	—

Even though higher G-CSF levels correlated with TNBC, not all TNBC cases demonstrated high levels of G-CSF. This might reflect the heterogeneity of TNBC, which has been reported to comprise six different subtypes displaying unique gene expression and ontology.²⁶ According to Lehmann et al., the MDA-MB-231 cell line represents the mesenchymal stem-like subtype whereas the Cal-51 cell line represents the mesenchymal type of breast cancer. Because the Cal-51 cell line did not induce HLA-DR^{lo} macrophages, we analyzed the secretion of G-CSF in Cal-51 cells. There was no detectable G-CSF in the conditioned medium of Cal-51 cells similar to the ER⁺ cell lines (Fig. 4D), which further confirms the importance of G-CSF in polarizing immunosuppressive macrophages.

In contrast to Cal-51 cells, the MDA-MB-231 cells have a KRAS mutation that leads to constitutive activation of the Ras-Raf-MEK-ERK pathway,²⁶ which may increase G-CSF secretion.²⁷ Indeed, selective inhibition of MEK1/2 in MDA-MB-231 cells by RDEA119 resulted in a significant reduction in G-CSF secretion after 24 h compared to the DMSO control (Fig. 4E; $p < 0.0001$). At this time point, no significant effect on cell viability was seen (Fig. 4E). After 48 h, G-CSF was undetectable in the RDEA119 treated MDA-MB-231 cells but also cell viability was decreased significantly (Fig. 4E; $p < 0.0001$).

High G-CSF expression in triple-negative breast cancer patients is associated with an abundance of CD68⁺CD163⁺ macrophages and TGF- α ⁺ cells

To investigate the possible effects of high G-CSF expression on the phenotype of TAMs, we analyzed the TAMs in the high and low G-CSF expressing TNBC. We stained the same tissue arrays for TAMs using antibodies against CD68 (Fig. 4F) and the widely used M2 macrophage marker CD163 (Fig. 4G). We chose to use CD163 instead of MR since we did not see a clear upregulation of MR on tumor-conditioned macrophages, and CD163 expression on TAMs has been reported to associate with poor prognosis in human breast cancer.²⁸ CD163 staining significantly correlated with CD68 staining (Fig. 4F; $p < 0.0001$), indicating that the CD163⁺ cells were indeed macrophages. Among the TNBC patients, we found more CD163⁺ cells in the high G-CSF expressing tumors than in the low G-CSF expressing tumors (Fig. 4G; $p < 0.0001$), suggesting that G-CSF might have a local effect in supporting M2-like macrophages in human breast cancer. High G-CSF expressing tumors also demonstrated a significantly higher number of TGF- α ⁺ cells (Fig. 4H; $p = 0.0069$). The analysis for TGF- α ⁺ cells was done on whole sections to have a more detailed analysis of the number and location of these cells. Interestingly, most of the TGF- α ⁺ cells resided in the invasive area in close vicinity to large blood vessels.

G-CSF and M-CSF differentiated macrophages show similar phenotypes with the exception of CD16 expression

To specify the human monocyte population responding to G-CSF signals, we measured the cell surface expression of G-CSF receptor (G-CSFR) on three different monocyte populations based on the expression of CD14 and CD16 by flow cytometry. G-CSFR was expressed on the surface of approx. 20% of the

classical CD14⁺CD16⁻ monocytes and was reduced gradually upon monocyte maturation (CD16⁺) (Fig. 5A). When stimulated with G-CSF, however, the CD14⁺CD16⁻ cells significantly upregulated CD16 expression compared to M-CSF or 1% normal human (AB) serum treated monocytes at day 5 (Fig. 5B; $p = 0.0081$), indicating that G-CSF promoted monocyte maturation into non-classical resident CD16⁺ macrophages. Both G-CSF and M-CSF increased cell surface MR

expression when compared to 1% AB serum but G-CSF was more effective than M-CSF at the same concentration (Fig. 5B; $p = 0.007$). No significant changes were observed in the cell surface expression of CD11c and CD86 (Fig. 5B); however, G-CSF induced a slight but significant increase in CD80 expression compared to 1% AB serum treated macrophages (Fig. 5B; $p = 0.0081$). Morphologically, the G-CSF-treated macrophages represented a more homogenous population than the M-CSF

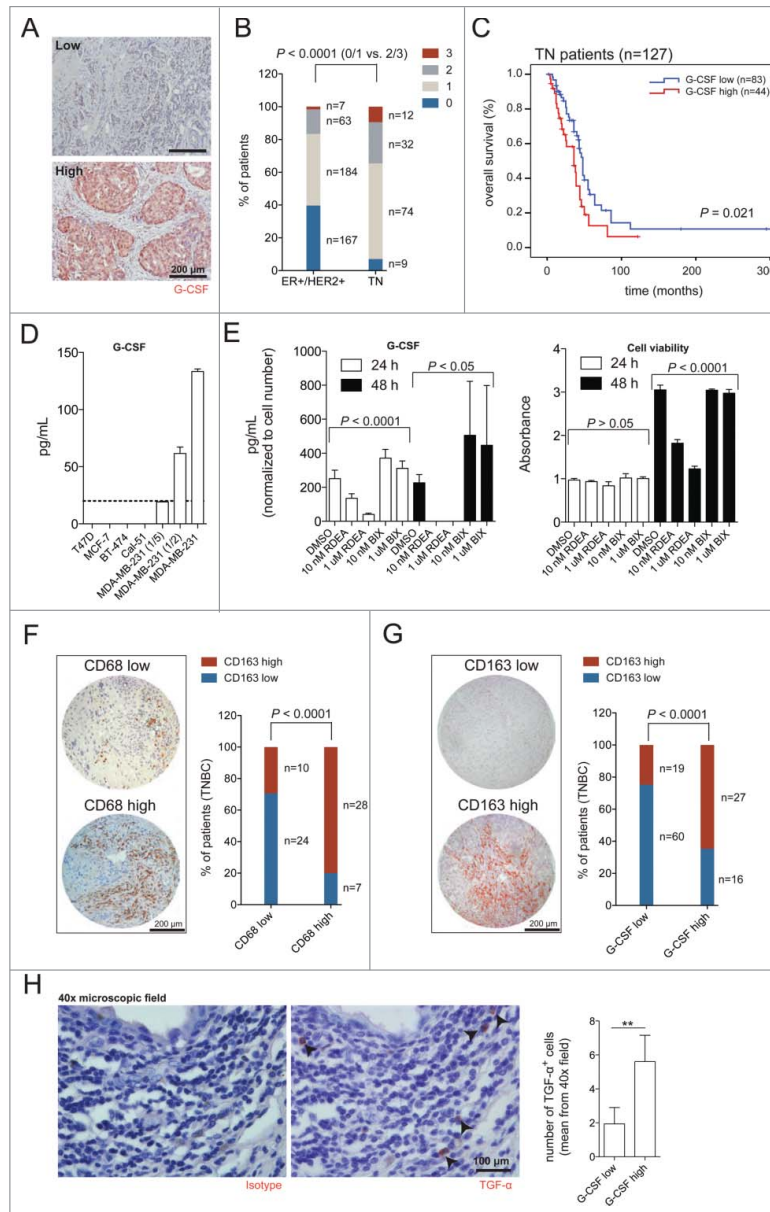


Figure 4. High G-CSF expression is significantly associated with CD163⁺ TAMs and decreased overall survival in human TNBC. (A) Representative images of G-CSF staining from invasive tumor area (low staining intensity 0/1; high staining intensity 2/3) with hematoxylin and eosin counter staining (H&E). (B) Quantification of G-CSF expression (staining intensity 0, 1, 2, 3) in ER⁺/HER2⁺ and triple-negative (TN) human breast cancer. The brackets above the graph represent statistical analysis between ER⁺/HER2⁺ and TN groups using *Chi*-square test. (C) Kaplan–Meier curves of overall survival (OS) in TNBC patients expressing low G-CSF (0/1) vs. high G-CSF (2/3) (Log-Rank test). (D) ELISA analysis of G-CSF levels on cancer conditioned medium of T47D, MCF-7, BT-474, Cal-51 and MDA-MB-231 cells. 1/2 and 1/5 indicate the dilutions of MDA-MB-231 CM. Error bars represent intra-assay variation between duplicate samples. The dashed line at 20 pg/mL represents the detection limit of the assay. (E) ELISA analysis of G-CSF levels and the corresponding cell viability of MDA-MB-231 cells after a 24- and 48-h incubation with the MEK1/2 inhibitor (RDEA) or MEK5 inhibitor (BIX). The G-CSF levels obtained from each well were normalized to cell viability to exclude the effect of cell number changes in G-CSF levels. The data is combined from three to four experiments performed in triplicates and analyzed using one-way ANOVA. (F) Representative images of low and high CD68 staining and statistical analysis of CD163 expression in association with CD68 low and high patients using *Chi*-square test. (G) Representative images of low and high CD163 staining and statistical analysis of CD163 expression in association with G-CSF low and high patients using *Chi*-square test. Two observers blinded to the identity of the samples performed the scoring of G-CSF samples independently. (H) Representative images of TGF- α staining in whole tumor sections. The arrowheads indicate positive cells. The number of TGF- α positive cells in 5–10 40x microscopic fields were quantified from 5 G-CSF low and 5 G-CSF high patients and means are shown in the graph. Statistical significance was analyzed using two-tailed Student’s *t*-test.

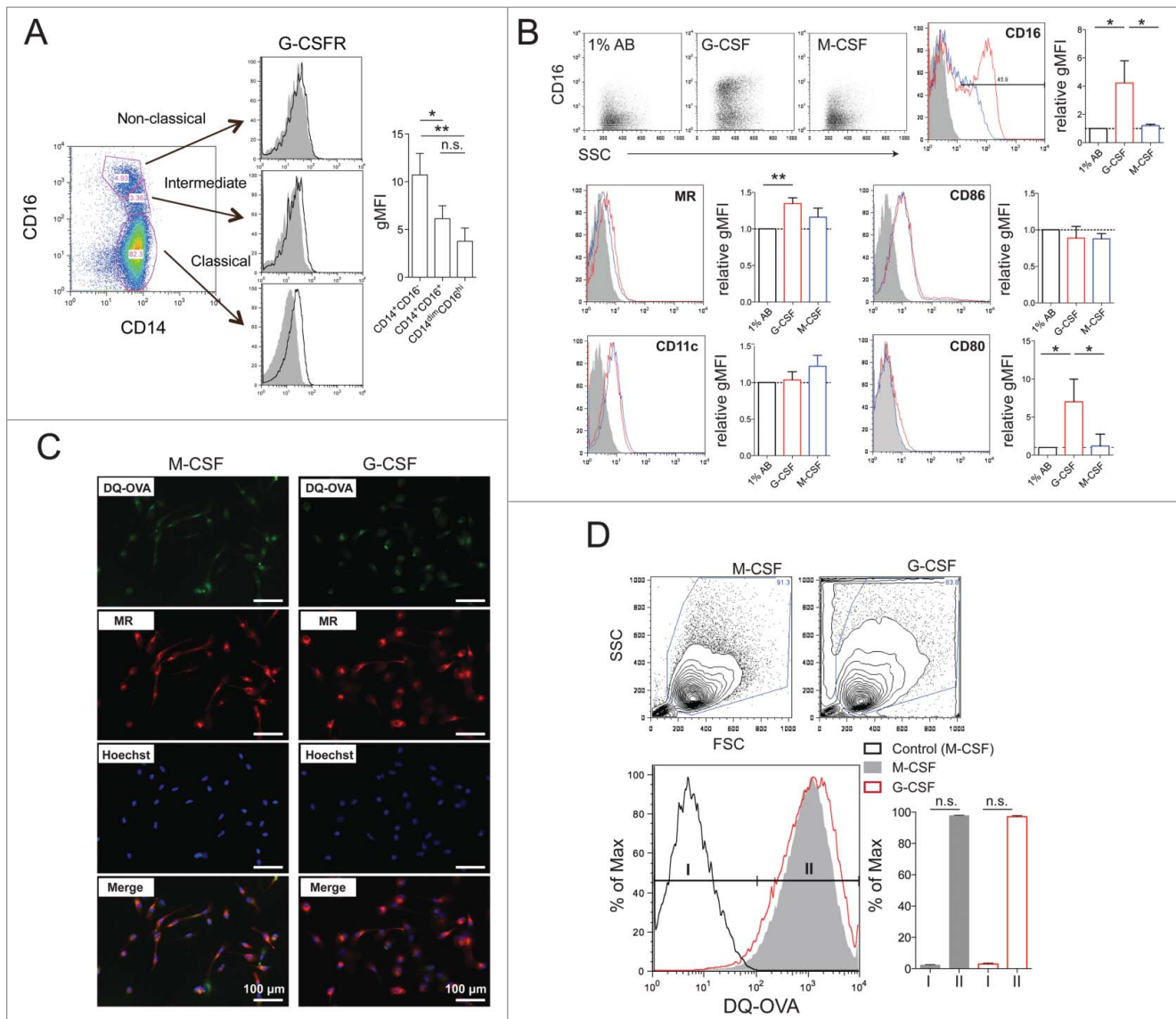


Figure 5. G-CSF- and M-CSF-differentiated macrophages show similar activation. (A) Flow cytometric analysis of cell surface G-CSFR expression on classical (CD14⁺CD16⁻), intermediate (CD14⁺CD16⁺) and non-classical (CD14^{dim}CD16^{hi}) human peripheral blood monocytes presented as geometric mean fluorescence intensity normalized to isotype control (gMFI; $n = 3$); one-way ANOVA with Tukey's multiple comparison test. (B) Flow cytometric analysis of cell surface expression levels of activation markers CD16 (maturation), MR (M2), CD86 (M1), CD11c (M1), and CD80 (M1) on human monocytes differentiated with 50 ng/mL G-CSF or M-CSF for 8 d. The gray-filled line shows the isotype control in the histograms. The expression levels of each marker in the graphs are presented as gMFIs and shown relative to the expression obtained from 1% AB serum treated monocytes from each donor ($n = 3$), one-way ANOVA with Tukey's multiple comparison test. (C) Immunofluorescence images of M-CSF and G-CSF differentiated human macrophages (day 8) treated with DQ-ovalbumin 2 h before fixation (green) and stained for MR (red). (D) Flow cytometric analysis of DQ-ovalbumin processing in M-CSF and G-CSF treated macrophages at day 8. The control (M-CSF) indicates cells that were differentiated with M-CSF but not treated with DQ-ovalbumin. I, negative for DQ-OVA; II, positive for DQ-OVA.

treated macrophages (Fig. 5C). Because only a subpopulation of monocytes expressed G-CSFR, cell death during macrophage differentiation using G-CSF was observed. No significant difference was seen in the ability to process fluorescently labeled ovalbumin (Fig. 5D).

Both G-CSFR and CSF-1R are expressed on tumor-induced CD11bLy6C⁺Ly6G⁺ myeloid cells and systemic CSF-1R blockade promotes metastasis in the 4T1 mammary tumor model

The effect of G-CSF on human monocytes prompted us to investigate how TAMs respond to high levels of G-CSF when the M-CSF/CSF-1R signaling route is inhibited *in vivo*. To this

end, we used the well-established 4T1 mammary tumor model²⁹ that is known to secrete high levels of G-CSF.³⁰ Administration of 10 mg/kg of anti-CSF-1R every second day promoted tumor growth (Fig. 6A; $p = 0.0005$) and enhanced metastasis to the draining inguinal ($p = 0.032$) and axillary ($p = 0.0063$) lymph nodes as well as to the lung ($p = 0.0083$) compared to control IgG-treated mice (Fig. 6B). In this setting, the anti-CSF-1R antibody prevented M-CSF from binding to CSF-1R because the serum levels of M-CSF increased substantially compared to control IgG-treated mice (Fig. 6C; $p < 0.0001$). Interestingly, both monocyte ($p = 0.012$) and neutrophil ($p = 0.0047$, data not shown) populations were increased in the blood of anti-CSF-1R treated mice compared to control mice (Fig. 6D). The anti-CSF-1R did not reduce the number of

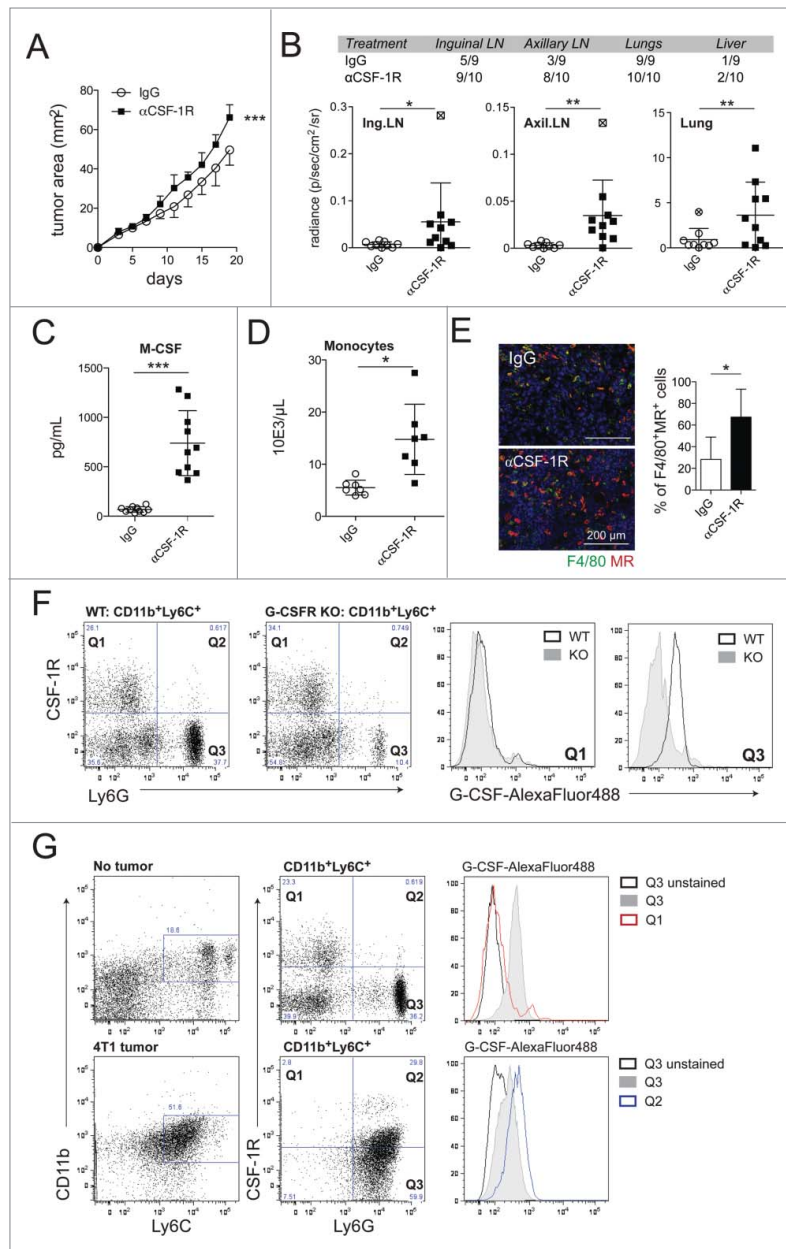


Figure 6. Anti-CSF-1R treatment promotes metastasis in the 4T1 model. (A) Growth curves of 4T1-luc mammary tumors treated with anti-CSF-1R ($n = 10$) or IgG control ($n = 9$) (both $200 \mu\text{g}/\text{mouse}$ every second day), two-way ANOVA. (B) On the day of sacrifice, the lymph nodes, lung and liver were dissected from the treated mice 10 min after a luciferin substrate injection and were imaged for metastatic burden using IVIS. The table shows metastasis positive organs on a yes/no basis, based on the IVIS signal and are shown as metastasis positive/total number of mice. The lower graphs show the radiance signal for each organ. Significant outliers were excluded from statistical analyses based on Grubbs' test and have been marked with a cross. Statistical significance was analyzed using two-tailed Student's t-test with Welch's correction. (C) ELISA analysis of serum M-CSF levels from mice treated either with IgG or anti-CSF-1R, two-tailed Student's t-test. (D) End point hematological analysis of monocytes analyzed with Sysmex XT-2000iV in IgG and anti-CSF-1R-treated mice. (E) Immunofluorescence staining of tumor sections (peritumoral area) with anti-F4/80 (green) and anti-MR antibodies (red) in IgG and anti-CSF-1R-treated mice. Quantification of double positive cells was done using ImageJ of three to five microscopic fields/mouse/treatment and analyzed using two-tailed Student's t-test. (F) Flow cytometric analysis of cell surface CSF-1R and G-CSFR expression on peripheral blood $\text{CD11b}^+\text{Ly6C}^+$ myeloid cells in C57BL/6 wild type (WT) and G-CSFR knockout (KO) mice where gate Q1 represents the monocytic population (Ly6C^-) and gate Q3 the granulocytic population (Ly6C^+). Because we used human recombinant G-CSF conjugated with AlexaFluor488 (G-CSF-488) for the detection of G-CSFR, the G-CSFR KO mice served as a control for specific binding of the protein. The histograms show binding of G-CSF-488 to the monocytic and granulocytic populations in WT (black line) and KO (gray-filled line) mice. (G) Flow cytometric analysis of cell surface CSF-1R and G-CSFR expression on peripheral blood $\text{CD11b}^+\text{Ly6C}^+$ myeloid cells in Balb/c mice without tumors or carrying a 4T1 tumor (size $5 \times 5 \text{ mm}$). As in (F), the Q3 gate served as a positive cell population for G-CSFR expression, and is shown as the gray-filled histograms. Note that the 4T1 tumor induced a granulocytic cell population double positive for CSF-1R and G-CSFR (Q2).

peritumoral F4/80^+ macrophages and these macrophages were also highly MR positive (Fig. 6E; $p = 0.021$).

To investigate which cell populations were targeted by anti-CSF-1R treatment, we analyzed both CSF-1R and G-CSFR cell surface expression on peripheral blood myeloid cells in non-tumor-bearing and 4T1 tumor-bearing mice. For the detection

of G-CSFR, we used an approach previously reported by Mitsui et al., where human recombinant G-CSF was conjugated and used in flow cytometry for the detection of mouse G-CSFR.³¹ To verify specific binding of the conjugated G-CSF to its receptor, we stained the $\text{CD11bLy6C}^+\text{Ly6C}^-$ monocytes (Q1) and $\text{CD11bLy6C}^+\text{Ly6C}^+$ granulocytes (Q3) from peripheral blood of

G-CSFR wild type (WT) and knockout (KO) mice (Fig. 6F). The KO mice clearly had a reduction of the number of Ly6G⁺ cells, verifying the KO phenotype. The KO granulocytes did not bind the conjugated G-CSF, in contrast to the WT granulocytes, indicating proper binding of G-CSF (Fig. 6F).

CSF-1R expression in non-tumor mice was only detected on Ly6C⁺Ly6G⁻ monocytes. These cells were also slightly positive for G-CSFR (Fig. 6G, upper panels). Surprisingly, the tumor-bearing mouse population consisted only of Ly6C⁺Ly6G⁺ cells that remained CSF-1R^{int/hi} and had increased expression of G-CSFR (blue line, Q2) compared to CSF-1R⁻ granulocytes (gray-filled line, Q3) (Fig. 6G, lower panels).

Blockade of both CSF-1R and G-CSF promotes inflammatory TAMs and reduces lung metastasis but promotes lymph node metastasis via depletion of CD169⁺ subcapsular sinus macrophages

Anti-G-CSF treatment in the 4T1 model has been previously shown to reduce peripheral mobilization of CD11b⁺Gr1⁺ cells and reduce metastasis to the lung.^{32,33} In our model, we observed a slight decrease in tumor growth when anti-G-CSF (0.6 mg/kg) treatment was administered every second day (Fig. S3A; $p < 0.05$ day 21). This anti-G-CSF treatment regimen resulted in an almost complete neutralization of G-CSF within the serum of tumor bearing mice (Fig. S3B; $p < 0.0001$). Moreover, the tumor-induced mobilization of blood monocytes ($p = 0.0002$) and neutrophils ($p < 0.0001$) was normalized by anti-G-CSF treatment (Fig. S3C). *Ex vivo*-isolated TAMs from anti-G-CSF-treated mice were almost completely negative for intracellular MR and showed the typical morphology of M1 macrophages (Fig. S3D). The anti-G-CSF-treated TAMs also processed fluorescently labeled ovalbumin more efficiently (Fig. S3E), which was seen as a significant rightward shift of the fluorescence intensity in the cumulative frequency plot (Fig. S3E; $p < 0.0001$). Since the anti-G-CSF treatment also reduced Gr1⁺ cells in the tumors and lungs (Fig. S3F), we specifically depleted Ly6G⁺ cells from the 4T1 tumor mice (Fig. S4A) to exclude the effects of Ly6G neutrophils on tumor promotion during anti-G-CSF therapy. Tumor growth (Fig. S4B) and metastasis (Fig. S4C) were not changed after depleting the Ly6G⁺ cells compared to the IgG controls.

We next treated the tumor-bearing mice with a combination of anti-G-CSF and anti-CSF-1R to specifically determine how G-CSF induced metastasis when CSF-1R was inhibited. We increased the dose of anti-G-CSF to 1 mg/kg since anti-CSF-1R treatment has been reported to increase G-CSF levels in the 4T1 model.³⁴ Anti-G-CSF as a single agent significantly reduced tumor growth (Fig. 7A; $p = 0.0007$), lung metastasis incidence ($p = 0.01$) and burden ($p = 0.048$) compared to IgG control mice (Fig. 7B). Blockade of both G-CSF and CSF-1R did not reduce primary tumor growth (Fig. 7A) but partly reduced lung metastasis incidence (Fig. 7B). Unexpectedly, the mice that received the combination treatment demonstrated significantly increased metastasis to the tumor-draining LNs compared to the other treatments (Fig. 7B; inguinal lymph nodes $p = 0.027$, axillary lymph nodes $p = 0.0075$).

Within the peripheral blood, anti-G-CSF and combination (anti G-CSF and anti-CSF-1R) treatment reduced the number

of CD11b cells (Fig. 7C; $p = 0.0009$) and normalized monocyte maturation compared to anti-CSF-1R only (Fig. 7C; red gates, Ly6C^{int} $p = 0.0003$, Ly6C^{lo} $p = 0.0006$). However, the combination treatment did not induce MHCII expression on Ly6C^{int/hi} monocytes, as did anti-G-CSF (Fig. 7C; blue gates, Ly6C^{hi} $p = 0.0002$, Ly6C^{int} $p = 0.0006$), indicating that the inflammatory monocyte population could not be activated when both signals were omitted. The combination treatment also significantly reduced the number of Ly6C^{lo}MHCII^{lo} anti-inflammatory TAMs compared to anti-CSF-1R treatment (Fig. 7D; red gates, $p = 0.0005$). Interestingly, anti-G-CSF treatment induced three TAM populations, one with Ly6C^{int}MHCII^{lo} expression (Fig. S5B). This population was the only one that showed a difference in the expression levels of F4/80 and MR between the different treatments. The F4/80 and MR expression on this population was promoted by G-CSF since the induction of F4/80 expression by anti-CSF-1R treatment could be blocked by the combination treatment (Fig. 7D; blue gates, F4/80 $p = 0.035$, MR n.s.).

These results suggest that there are different mechanisms that facilitate lung metastasis in comparison to LN metastasis. This was evident from the different patterns that were seen either when G-CSF or CSF-1R was inhibited. Since anti-CSF-1R treatment also targets macrophages outside of tumors, we investigated the effects of anti-CSF-1R on CD169⁺ subcapsular sinus macrophages. We observed a depletion of CD169⁺ cells in the subcapsular sinus area in all LNs treated either with anti-CSF-1R or combination treatment (Fig. 7E), possibly facilitating tumor cell entry into the lymph node tissue in the absence of the gatekeeper macrophages.

Discussion

In this study, we identify an important role for G-CSF in modulating the phenotype of anti-inflammatory monocytes and TAMs in both human and mouse tumors. While the ER⁺ and HER2⁺ subtype of human breast cancers demonstrated low levels of G-CSF staining, TNBC with high levels of G-CSF were associated with increased CD163⁺ macrophage numbers and decreased OS compared to low G-CSF expressing tumors. Our data are in accordance with reports indicating that—apart from its beneficial effect—G-CSF also mediates T-cell tolerance,³⁵ suppression of dendritic cell differentiation,³⁶ and facilitates neoplastic growth,³⁰ metastasis³² and refractoriness to anti-VEGF treatment³³ through a granulocytic myeloid-derived suppressor cell mechanism. High levels of tumor-secreted G-CSF have been reported in some sporadic cases of aggressive human tumors³⁷⁻³⁹ and more recently, high expression of G-CSF and G-CSFR was reported in colon and gastric cancer, where G-CSF promoted carcinoma cell proliferation and migration.⁴⁰

Elevated G-CSF secretion in human TNBC most likely arises from the different activation of driver mutations in these tumors that are not present in ER⁺ breast cancers. For example, mouse breast cancer cell lines with constitutive activation of the Ras-Raf-MEK pathway produce pronounced amounts of G-CSF.²⁷ Since we did not detect high G-CSF in the conditioned medium of the Cal-51 cell line and G-CSF was also heterogeneously expressed among the TNBC patients, we propose that

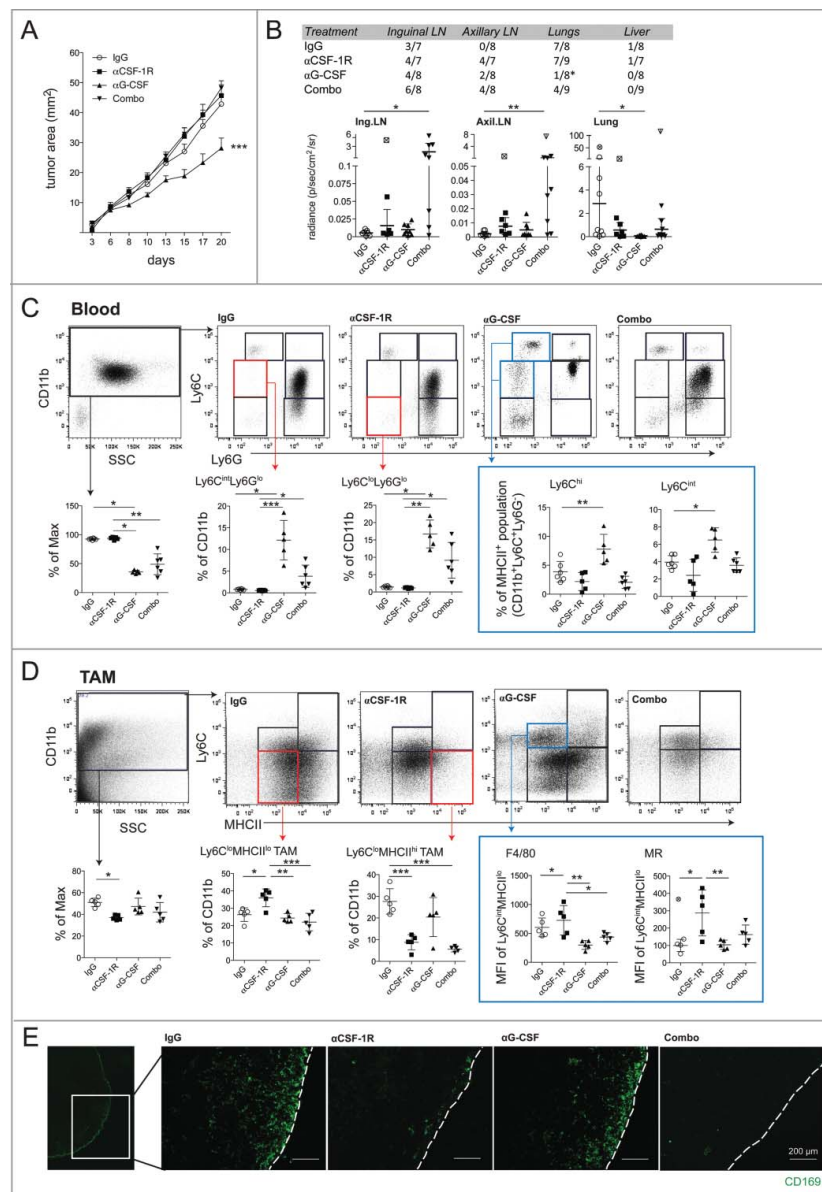


Figure 7. Combination treatment of blocking both CSF-1R and G-CSF reduces lung metastasis but promotes lymph node metastasis via depletion of CD169⁺ subcapsular sinus macrophages. (A) Growth curves of 4T1.1A4-luc mammary tumors treated with IgG control ($n = 8$, 220 μ g/mouse), anti-CSF-1R ($n = 7$, 200 μ g/mouse), anti-G-CSF ($n = 8$, 20 μ g/mouse) or combination treatment ($n = 9$, anti-CSF-1R 200 μ g/mouse and anti-G-CSF 20 μ g/mouse). Statistical analysis was done using two-way ANOVA. (B) On the day of sacrifice, the lymph nodes, lung and liver were dissected from the treated mice 10 min after a luciferin substrate injection and imaged for metastatic burden using IVIS. The upper numbers show metastasis positive organs on a yes/no basis based on the IVIS signal and are shown as metastasis positive/total number of mice. The asterisk indicates significant reduction in metastasis compared to IgG control and was analyzed using Fisher's exact test. The lower graphs show the radiance signal for each organ. Significant outliers were excluded from statistical analyses based on Grubbs' test and have been marked with a cross. (C) The effect of the different treatments on blood myeloid cell populations in tumor bearing mice were analyzed by flow cytometry based on CD11b⁺ and further gated for monocytic cell populations using Ly6C and granulocytic cell populations using Ly6G. The anti-G-CSF plots were used for the gating strategy of the different blood myeloid cell populations since it normalized blood monocytic cell differentiation (Ly6C^{int-lo}; see also Fig. S5A). From this gating strategy, the gates marked as red show detailed analysis of five mice/treatment for the percentage of CD11b cells in these gates (Ly6C^{int}Ly6G^{lo} and Ly6C^{hi}Ly6G^{lo}). The gates marked as blue show detailed analysis of cell surface MHCII expression on Ly6C^{hi} and Ly6C^{int} monocytes between treatments. (D) Different TAM populations were analyzed using the gating strategy previously reported by Movahedi et al.,⁵² where CD11b⁺ cells are gated further using Ly6C and MHCII to identify anti-inflammatory TAMs (Ly6C^{int}MHCII^{lo}) and pro-inflammatory TAMs (Ly6C^{int}MHCII^{hi}). The gates marked as red show detailed analysis of five mice/treatment for the percentage of CD11b that have low and high MHCII expression. The anti-G-CSF treated TAMs formed a population of Ly6C^{int}MHCII^{lo} cells (blue gate) that were further analyzed for the expression of activation markers F4/80 and MR (mean fluorescence intensity, MFI) between treatment groups. (E) Immunofluorescence images of lymph nodes stained with anti-CD169 (green) to identify the effect of the different treatments on subcapsular sinus macrophages. The white-dashed line indicates the LN border. All statistical significances were tested using one-way ANOVA with Tukey's multiple comparison test unless otherwise stated.

only a part of cells with acquired KRAS mutation may have the ability to produce pathological amounts of G-CSF, which importantly can be targeted by inhibiting Ras downstream signaling using the MEK1/2 inhibitor. The fact that normal mammary glands also expressed G-CSF highlights the possibility that different mechanism(s) exist for the secretion of G-CSF

from TNBC and non-malignant cells. One possibility is the difference in microenvironments where G-CSF is present, such that in TNBC other stromal cells and secreted molecules contribute to enforce the immunosuppressive activity of G-CSF. Another possibility is alternative splicing of the CSF3 gene, which generates at least three different forms of the G-CSF

protein.⁴¹ This might lead to different soluble or membrane bound forms of G-CSF that have different activities on stromal compartments, similar to what has been reported for M-CSF.⁴²

In our study, G-CSF differentiated CD14⁺ monocytes expressed lower levels of HLA-DR and inhibited CD4⁺ T-cell activation in response to tetanus toxoid. These cells were also able to promote migration of Cal-51 cells via secretion of TGF- α . The effect of G-CSF in activating TGF- α secretion was further supported by our clinical data where a significantly higher number of TGF- α ⁺ single cells were found in tumors with high expression of G-CSF. The MDA-MB-231 produced G-CSF did not activate TGF- α secretion similar to the recombinant protein, which might result from the lower levels of G-CSF in MDA-MB-231 CM (5.5 ng/mL) vs. recombinant G-CSF (40 ng/mL). The MDA-MB-231 CM contains also many other factors that might inhibit TGF- α upregulation on macrophages directly or indirectly via other signaling molecules. Along with this notion, the multitude of molecules secreted by MDA-MB-231 cells might activate macrophages to secrete molecules that can also be chemotactic for T47D since a migratory response of T47D cells to MDA-MB-231 CM differentiated macrophages was observed.

TGF- α is a growth factor that binds the EGFR and activates several pathways (PI3K-Akt-mTOR and Ras-Raf-MEK-ERK) that mediate cell proliferation, migration, invasion and angiogenesis. EGFR is more commonly expressed by basal-like and TNBC cancers⁴³ and associates with low hormone status, higher proliferation, genomic instability and reduced disease-free survival.⁴⁴ Our analysis of EGFR expression in ER⁺ and TNBC cell lines demonstrated that only Cal-51 and MDA-MB-231 cells expressed detectable amounts of EGFR. Thus, both cell lines are able to respond to macrophage secreted TGF- α . The MDA-MB-231 cell line, however, does not need reinforcement of EGFR signaling by TGF- α since the Ras pathway is constitutively activated. As the Cal-51 cells did not basally secrete G-CSF, it remains to be investigated whether these cells would upregulate G-CSF when activated by TGF- α . There could also exist a “parallel” paracrine signaling loop where secretion of G-CSF by one type on cancer cell would end up activating another type of cancer cell with EGFR expression. Since many other tumor stromal components can secrete G-CSF,⁴⁵ the induction of TGF- α expression by macrophages may not necessarily be always cancer cell driven. This notion also raises the possibility that G-CSF therapy used to treat febrile neutropenia of some breast cancer patients may have adverse effects in promoting tumor cell migration via activation of TAMs to secrete TGF- α .

M-CSF is the major growth factor for blood monocytes to mature into tissue macrophages and has been extensively studied as a drug target. We found that inhibiting the M-CSF/CSF-1R signaling axis in the 4T1 model significantly increased metastasis to the tumor draining LN and lung. A recently published study described similar findings after antibody or small molecule based targeting of M-CSF and CSF-1R in the 4T1.2 and EMT6.5 breast cancer models.³⁴ In this paper, the authors concluded that the increased lung metastasis might have been a result of increased G-CSF mediated recruitment of neutrophils and Ly6C^{hi} monocytes in the peripheral blood because no changes of TAM numbers were observed. Our study now shows that, indeed, G-CSF potentially mediated metastasis to the lung via

recruitment of anti-inflammatory Ly6C^{hi/int}MHCII^{lo} peripheral blood monocytes. Additionally, we show that G-CSF mediates differentiation of Ly6C^{lo}MHCII^{lo} anti-inflammatory TAMs when CSF-1R is inhibited. This suggests that in the presence of high G-CSF, the tumor-recruited monocyte populations are not dependent on M-CSF for their survival and differentiate according to G-CSF-generated anti-inflammatory cues. This goes along with our observation that tumor-induced mouse myeloid cells express both CSF-1R and G-CSFR in contrast to the normal situation where CSF-1R is expressed solely on CD11bLy6C⁺Ly6G⁻ and G-CSFR mainly on CD11bLy6C⁺Ly6G⁺ cells. Depletion of Ly6G⁺ cells did not significantly affect primary tumor growth or metastasis to the inguinal and axillary lymph nodes and lungs. Also, Granot and colleagues showed that G-CSF induced neutrophils do not have any effect on lung foci formation in an experimental metastasis model.⁴⁶ They also showed that depletion of Ly6G⁺ increased metastasis to the lung rather than inhibited it. Thus, we conclude that the effects of G-CSF in promoting metastasis would be orchestrated by M2-like macrophages and/or MHCII^{lo} anti-inflammatory monocytes.

Importantly, we found a striking increase in LN metastasis burden in mice treated with anti-G-CSF in combination with anti-CSF-1R. We propose that the increased metastasis was promoted by the almost complete depletion of CD169⁺ subcapsular sinus macrophages in the tumor-draining LNs of the combination treated mice. In fact, a similar but subtler effect was seen already when anti-CSF-1R was used as a single agent, possibly indicating that CSF-1R is a major growth factor for subcapsular sinus CD169⁺ macrophages even in the presence of high levels of G-CSF. CD169⁺ macrophages are important gatekeeper cells lining the lymphatic endothelial wall on the subcapsular sinus where they prevent systemic pathogen dissemination. The importance of CD169⁺ macrophages in anti-tumor responses was demonstrated by Asano and colleagues⁴⁷ where mice lacking CD169⁺ macrophages in the tumor-draining LN failed to generate antitumor immunity via activation of tumor-specific CD8⁺ T-cells. Moreover, in human clinical samples, a high number of CD169⁺ macrophages in the regional LNs of colorectal carcinoma⁴⁸ and malignant melanoma patients⁴⁹ was associated with longer OS.

In conclusion, our results reveal that aggressive breast cancers secrete high amounts of G-CSF that educates tumor-infiltrating monocytes to promote tumor growth by skewing them to an anti-inflammatory phenotype with enhanced secretion of TGF- α (Fig. S5C). Therefore, patients with high G-CSF producing tumors might benefit from anti-G-CSF treatment to reduce Th2-activated myelopoiesis and inhibit metastatic seeding, which should be investigated in future clinical studies. Our results also indicate that tumor G-CSF levels should be taken into consideration when using M-CSF/CSF-1R blocking agents to deplete macrophages in breast cancer.

Materials and methods

Isolation of human peripheral monocytes and differentiation assays

Peripheral blood mononuclear cells were isolated from buffy coats from healthy donors (Blutspende Zürich, Zurich,

Switzerland) by density gradient centrifugation using Ficoll-paque PLUS (Cat: 17-1440-02; GE Healthcare). The monocyte population was magnetically enriched by negative selection using the Human Monocyte Isolation Kit II (Cat: 130-091-153; MACS, Miltenyi Biotech). The monocyte purity was >95% as confirmed by FACS analysis with an anti-CD14 antibody (BD Biosciences).

Freshly isolated human monocytes were differentiated into macrophages by incubation with either 50 ng/mL of human M-CSF (Cat: 14-8789) or G-CSF (Cat: 578602) (both from BioLegend) in RPMI medium (Cat: 61870-010; Gibco) supplemented with 1% heat-inactivated human AB serum (Cat: 34005100; Invitrogen), for up to 8 d. 20 ng/mL of recombinant human IL-4 (Cat: 204-IL; R&D Systems) was used as a control to induce M2-type macrophage differentiation and anti-human G-CSF (1 μ g/mL, clone BVD13-3A5, Cat: 502101; BioLegend) or isotype control (rat IgG1 Cat: 400401) was used to neutralize G-CSF in MDA-MB-231 conditioned medium.

Cell lines and conditioned media (CM)

T47D, SKBR-3 and MDA-MB-231 (kindly provided by Dr Nancy E. Hynes, FMI, Basel, Switzerland), MCF-7, BT-474 and Cal-51 (kindly provided by Prof. Pirkko Härkönen, University of Turku, Turku, Finland) were maintained in RPMI medium supplemented with 10% fetal bovine serum. According to published data, the T47D and MCF-7 cell lines are ER⁺HER2⁻, the BT-474 cells line is ER⁺HER2⁺, the SKBR-3 cell line is ER⁻HER2⁺, and the Cal-51 and MDA-MB-231 cell lines are ER⁻HER2⁻.^{26, 50} Before experimentation, all cell lines were tested negative for mycoplasma with MycoProbe (Cat: CUL001B; R&D Systems). To produce conditioned media (CM), cancer cells were plated at a density of 2×10^6 cells in 10 cm cell culture plates. The next day, cells were washed twice with PBS and incubated with RPMI medium only. Cell cultures or empty culture plates (control) were incubated at 37°C for 24 h. The medium was collected, filtered through a 0.22 μ m syringe and stored at -80°C if not used fresh.

Transwell co-culture assay

Cancer cells were seeded into the lower compartment of 12 well transwell PET permeable supports, pore size 0.4 μ m (Cat: 3470; Corning; 5×10^4 cells/well) and were incubated overnight in RPMI supplemented with 10% FBS. Then, cells were washed with PBS and incubated in RPMI for one hour before adding 5×10^4 freshly isolated human peripheral monocytes into the upper compartment of the transwell inserts. The co-cultures were incubated for up to 8 d in a humidified chamber at 37°C.

Immunofluorescence staining

Human monocytes/macrophages were fixed with methanol and stained with anti-CD68 (clone PG-MI, Cat: M 0876; Dako; 1:100) and anti-CD206 (MR) (clone 309210, Cat: MAB2534; R&D Systems; 1:100) antibodies diluted in Antibody Diluent (Zytomed Systems). The signal was detected using Alexa Fluor

488 and 594 conjugated secondary antibodies (Molecular Probes) and the samples were imaged with an Axioskop 2 mot plus fluorescence microscope equipped with Plan-APOCHROMAT 20 \times /0.8 NA and 40 \times /0.95 NA objectives and an Axio-Cam MRc camera with AxioVision software 4.7.1 (Carl Zeiss AG). The staining intensity was quantified using ImageJ software and the percentage of CD68⁺ cells that were also MR-positive was determined.

Frozen tumors sections (7 μ m) were stained with anti-F4/80 (clone C1:A3-1, Cat: ab6640; Abcam; 1:100) and anti-MR (Cat: AF535; R&D Systems; 1:250) antibodies, and tumor-draining LNs with anti-CD169 antibody (clone 3D6.112, Cat: MCA884F; Serotec; 1:100) as described above.

Flow cytometric analysis of activation markers on monocytes/macrophages

Human monocytes/macrophages were cultured either in ultra-low attachment 96-well plates (1×10^5 cells, Cat: 7007; Corning) or in six-well plates (5×10^5 cells) in CM or in medium supplemented with M-CSF and G-CSF up to 8 d. The adherent macrophages were detached using 10 mM EDTA in PBS and gentle scraping. Primary antibodies and the Fc-blocking anti-human antibody (Cat: 14-9161, eBioscience) were diluted in FACS buffer (PBS with 1% BSA and 2 mM EDTA). The pelleted cells were pre-incubated with the Fc-block for 10 min and thereafter stained with the following antibodies at 1:200 dilution for 30 min on ice in dark: CD14-Pacific blue or -FITC (clone M5E2, Cat: 558121 or 557153), CD16-PE (clone 3G8, Cat: 555407), MR-APC (clone 19.2, Cat: 550889), HLA-DR-FITC (clone Tu39, Cat: 555558), CD11c-PE (clone B-ly6, Cat: 555392) (all from BD Biosciences), CD86-FITC (clone BU63, Cat: MCA1118F, AbD Serotec) and CD114-PerCP/Cy5.5 (G-CSFR; clone LMM741, Cat: 346109; BioLegend). The cells were washed twice with FACS buffer and analyzed immediately with a FACS Canto or LSR Fortessa Flow Cytometer (Becton Dickinson and Company) using the FACS Diva software. FlowJo software (v9.3.2) was used to analyze the data. The expression levels of activation markers were reported as the difference between the geometric mean fluorescence intensity (gMFI) with a specific antibody and the isotype control gMFI.

Mouse monocytes/macrophages were stained as above using the CD16/CD32 Fc-block (clone 2.4G2, Cat: 553142; BD) and the following antibodies: CD45-PerCP-Cy5.5 (clone 30-F11, Cat: 550994; BD), CD11b-APC or -APC-Cy7 (clone M1/70, Cat: 553312 or 561039; BD), Ly6G-BV510 or -PE (clone 1A8, Cat: 127633; Biolegend or Cat: 551461; BD), Ly6C-BV421 (clone AL-21, Cat: 562727; BD), I-A/I-E-BV510 or -PE-Cy7 (clone M5/114.15.2, Cat: 107635; Biolegend or 25-5321-82; eBioscience), F4/80-Alexa647 (clone A3-1, Cat: MCA497A647; AbD Serotec), CD206-Alexa488, CD115-PE-Cy7 (clone AFS98, Cat: 25-1152-80; eBioscience) and analyzed with an LSR Fortessa Flow Cytometer (BD).

The recombinant human G-CSF was conjugated with Alexa Fluor 488 using the Alexa Fluor 488 microscale protein labeling kit (A30006, Molecular Probes) according to the manufacturer's protocol. The conjugated recombinant protein was used similar to the directly conjugated antibodies in flow cytometry.

Ovalbumin processing

DQ-Ovalbumin BODIPY FL (10 $\mu\text{g}/\text{mL}$, Cat: D12053; Molecular Probes) was added to cell cultures 2 h before fixing the cells with ice-cold methanol. For human macrophages, the intracellular processed ovalbumin was quantified on the basis of OVA positive/negative cells by fluorescence microscopy or by flow cytometry.

Multiplex assay and ELISA

Conditioned media (serum-free) were analyzed for cytokine, chemokine and growth factor production using Bio-plex pro assay Human Cytokine 21-plex (Cat: MF0-005KMII) and Human Cytokine 27-plex (Cat: M50-0KCAF0Y) (BioRad) according to the manufacturer's instructions.

G-CSF levels in conditioned media of 4T1 cells and in mouse serum samples were measured according to the manufacturer's instructions (Cat: ELM-GCSF; RayBiotech) at a 1:50 dilution. Human G-CSF was measured in undiluted cancer cell CM using the Human G-CSF Quantikine ELISA-component kit (Cat: DCS50, R&D Systems). TGF- α (Cat: 100646) and oncostatin M (OSM, Cat: ab100619) levels in human monocyte/macrophage conditioned media (undiluted) were measured using human ELISA kits according to the manufacturer's instructions (Abcam).

Tetanus toxoid response in CD4⁺ T cells

Monocytes (positive selection, CD14 monocyte enrichment kit, Miltenyi Biotech) and CD4⁺ T-cells (negative selection, CD4⁺ T-cell enrichment kit, EasySep) were enriched from the same donors vaccinated within the past 3 y with tetanus toxoid. The monocytes were isolated 4 d prior to T cells to differentiate them either with 1% human serum or 50 ng/mL of G-CSF in low attachment 96-well culture plates. On the day of T-cell isolation, the differentiated monocytes were plated at a density of 3×10^4 cells in 96-well flat bottom plates and let to adhere for one hour. The monocytes were then pulsed with 20 $\mu\text{g}/\text{mL}$ of tetanus toxoid (a kind gift from Dr Olli Lassila, Department of Medical Microbiology, University of Turku, Turku, Finland) 3 h prior to the addition of 3×10^5 of CFSE-labeled CD4⁺ T cells in a medium containing RPMI, 10% FCS, 2 mM L-glutamine and 100 μM β -mercaptoethanol. For labeling T cells with CFSE (Vybrant CFDA SE cell tracer kit, Cat: VI2883, Molecular Probes), a concentration of 1 μM CFSE for 5 min at 37°C for 1×10^6 cells/mL was used.

96-well ELISpot plates (Mabtech) were coated with anti-human IFN γ (1 $\mu\text{g}/\text{mL}$) for 2 h at 37°C, washed with PBS and blocked with 10% FCS in RPMI. The enriched monocytes and CD4⁺ T cells were co-cultured in the precoated ELISpot wells in triplicates at a ratio of 1:10 (1×10^4 monocytes and 1×10^5 T-cells). After three days, the wells were washed and incubated with biotinylated anti-IFN γ and alkaline phosphatase-conjugated anti-biotin secondary antibody (1:1000). Spots were developed with BCIP/NBT solution and counted microscopically. The number of spots from tetanus toxoid activated co-cultures were normalized to the spot count of wells containing T cells only, T cells with tetanus toxoid and T cells with monocytes but without tetanus toxoid.

Migration assay

Freshly isolated monocytes (5×10^4) were incubated in 24-well plates with 1% AB serum, T47D CM, MDA-MB-231 CM, or 40 ng/mL human recombinant G-CSF (Cat: 561701; eBiosciences) in 1% AB serum for 48 h. Thereafter, the cells were washed with PBS and incubated for 24 h in RPMI. After this, either 2×10^4 T47D or MDA-MB-231 cells were added on top of the polarized macrophages in collagen pre-coated transwell inserts with a pore size of 8 μm (Corning). The transwell inserts were coated according to the protocol from Corning with Type I Collagen Solution from Rat Tail (Cat: C3867; Sigma). The cells were let to migrate for 6 h. The migrated cells were visualized by Hoechst staining and counted under a microscope in five different visual fields per insert. Each condition was done in triplicates.

Western blot

SDS-PAGE and Western blotting for EGFR detection (sc-03, 1:1000 dilution; Santa Cruz) on cancer cell lysates (50 $\mu\text{g}/\text{well}$) was performed using standard procedures. The anti-EGFR signal was detected using IRdye680 donkey anti-rabbit (Cat: 925-68073; LiCOR) and imaged using the LiCOR Odyssey CLx system. Anti-tubulin (TUB 2.1, sc-58886; Santa Cruz) was used simultaneously as a loading control and detected by IRdye800 donkey anti-mouse (Cat: 925-32212; LiCOR). ChameleonDuo Pre-stained Protein Ladder (Cat: P/N 928-60000; LiCOR) was used as a protein standard.

Scratch wound healing assay

Cal-51 cells were plated on ImageLock 96-well plates (Cat: 4379, Essen Bioscience) as a confluent layer (4×10^4 cells). A scratch wound was made to each well the next day, using a 96-pin wound-making tool (Wound MakerTM, Essen Bioscience). The medium was replaced by CM collected from monocytes grown in control medium (RPMI only) or 50 ng/mL of G-CSF for 4 d and added as a 1:2 dilution in RPMI supplemented with 1% FCS. 5 $\mu\text{g}/\text{mL}$ of anti-TGF- α antibody (Cat: ab9585, Abcam) or isotype control (rabbit IgGs) was added to the CM before experimentation. Each condition was studied in triplicates. Anti-TGF- α antibody in medium supplemented with or without 10% serum in RPMI was found to have no effect on Cal-51 migration compared to isotype control. Cal-51 migration was scanned every 2 h with a 10x objective by the Incucyte ZOOM system (Essen Bioscience) for a total of 48 h at 37°C. Wound width was analyzed from the scanned images using the Essenbio software. The assay was performed using CM collected from three different donor monocytes.

Human samples

Human breast cancer tissue was obtained from the diagnostic service of the Institute of Surgical Pathology, University Hospital Zürich, Zurich, Switzerland. For large sections, 2 μm thick sections from 52 cases of paraffin embedded breast cancer samples with adjacent normal breast tissues were used. Tissue micro arrays (TMA) were constructed as described

previously.⁵¹ TMA21 contained breast cancer spots from 475 consecutive breast cancer cases and TMA174 contained 91 spots from hormone receptor negative breast cancers where 83 cases were also triple-negative. Patient demographic data of the TMAs are presented in Table S1. The study on human breast cancer tissues was approved by the local ethical committee (KEK-Nr. 2012–553) and by the internal review board of the Institute of Surgical Pathology, University Hospital Zürich, Zurich, Switzerland.

Immunohistochemical stainings

Human paraffin-embedded sections/tumor micro-arrays were stained with primary antibodies for G-CSF (Cat: ab9691, Abcam; 1:400), CD163 (clone 10D6, Cat: NCL⁺CD163, Novocastra; 1:50) or TGF- α (Cat: ab112030, Abcam; 1:300) using citrate buffer (pH 6) antigen retrieval, and for CD68 (clone PG-M1, Cat: M0876, DakoCytomation; 1:200) using EDTA pH 9.0 antigen retrieval, a 1:200 dilution of biotinylated anti-rabbit or mouse secondary antibodies, the ABC kit, and 3-amino-9-ethylcarbazole (AEC) peroxidase substrate (all from Vector Laboratories). The slides were evaluated and scored by two observers blinded to sample identity. If the two observers disagreed in scoring, the samples were re-evaluated by a third blinded observer. Scoring of G-CSF staining was done semi quantitatively as follows: score 0, no reactivity; score 1, weak cytoplasmic reactivity in < 50% of the tumor surface; score 2, moderate cytoplasmic reactivity in > 50% of the tumor surface; score 3, strong cytoplasmic reactivity in > 50% of the tumor surface. Representative staining areas from different scoring is shown in Fig. S2A. The scoring for CD68 staining was done with a cut-off of 30% stained area, low representing < 30% coverage and high representing ≥ 30 % coverage of the tumor-array spot.

MEK inhibitor treatment and cell viability assay

MDA-MB-231 cells were plated at a density of 1×10^4 cells in 96-well flat-bottom cell culture plates (Corning). The next day, the cells were starved for 4 h in RPMI medium only before the addition of 10 nM or 1 μ M of the MEK1/2 inhibitor RDEA119 (Cat: 1089), the MEK5 inhibitor BIX02189 (Cat: S1531) (both from Selleckchem) or a similar volume of DMSO for 24–48 h. The medium was collected for G-CSF ELISA analysis after 24 and 48 h and replaced by 100 μ L of RPMI containing 10 μ L of the CCK8 reagent (Cat: CK04–11, Dojindo) for cell viability analysis. All experiments were performed in triplicates with 3–4 repetitions. The G-CSF level for each well was normalized to the corresponding absorbance signal.

4T1 mammary tumors

All animal experiments were approved by the cantonal veterinary office Zurich (Kantonales Veterinäramt Zürich; protocol 11/2012) or The Finnish Act on Animal Experimentation (62/2006), performed in compliance with the 3Rs principle and accepted by the local Committee for Animal Experimentation (animal license number 5587/04.10.07/2014). The G-CSFR KO mice (B6.129X1(Cg)-Csf3r^{tm1Link}) were purchased from the

Jackson Laboratory. Heterozygous breeding of the mice generated the WT littermate controls.

For the tumor studies, 1×10^5 luciferase-expressing 4T1 (Caliper Life Sciences) or 4T1.1A4 cells (Xenogen) (used in combination study) were injected into the inguinal mammary fat pad of 8–10-week old female Balb/c mice (Charles River). Antibody treatment (i.p.) was started at day 3 after tumor inoculation and was given every second to third day until the end of the study with the following doses: anti-G-CSF 20 μ g/mouse (clone 67604, Cat: MAB414; R&D Systems), anti-CSF-1R 200 μ g/mouse (AFS98, Cat: BE0213; BioXCell), IgG from rat serum (Sigma) control 200 μ g/mouse in anti-CSF-1R and 220 μ g/mouse in combination study. Tumor size was measured with a digital caliper and calculated using the formula $T_{area} = \pi/4 \times \text{larger diameter} \times \text{smaller diameter}$. At the day of sacrifice, the mice were injected with 150 mg/kg of D-luciferin substrate (Caliper Life Sciences) and anesthetized after 5 min with a lethal dose (100 μ L) of Narketan-Domitor 4:1 solution (ketamine 400 mg/kg and medetomidine 10 mg/kg) or CO₂. The blood was collected by cardiac puncture for flow cytometry or hematological analyses with Sysmex XT-2000iV, a flow cytometry device based on a sheath-flow and a semiconductor laser for an optical method for assessing white blood cell counts and differentiation (Clinical Laboratory of Veterinary Medicine, University of Zurich, Zurich, Switzerland). The lungs, liver and lymph nodes were excised and imaged (IVIS) after 10 min with the following settings: exposure time = 10 seconds (lungs), 30 seconds (lymph nodes and liver), f/stop=1, medium binning, field of view = 3.9×3.9 cm². Living Image software was used to quantify the bioluminescent signal reported as units of tissue radiance (photons/s/cm²/sr).

Tumor digestion

Tumors were minced into 1–2 mm³ pieces and digested in digestion solution (10 mg/mL collagenase IV (Gibco), 20 μ g/mL DNase (Invitrogen), 2.25 μ M CaCl₂ in PBS) in a shaker heated to 37°C. After 30 min, the tissue was filtered through a 40 μ m cell strainer and flushed with 20 mL of MACS buffer (0.5% FBS, 2 mM EDTA in PBS). The single cell suspensions were analyzed for TAMs using flow cytometry.

Statistical analyses

Results are presented as mean \pm SD. Statistical significance was determined as indicated in the figure legends. The analyses were performed and the graphs plotted in Prism V5.0 (GraphPad Software), PASWStatistics 18.0 (SPSS Inc.) or Matlab version 7.12.0.635 R2011a (Mathworks Inc.). A *p* value of ≤ 0.05 was considered to be statistically significant. The results obtained using one-way ANOVA are presented by the ANOVA values in text and individual significances between groups are indicated by asterisks in the figures. Only the significant differences are indicated in figures by using * unless specifically marked as n.s. (not significant). **p* ≤ 0.05 ; ***p* ≤ 0.01 ; ****p* ≤ 0.001 .

Author contributions

MH developed the concept, designed, performed and analyzed the co-culture experiments, the G-CSF effects *in vitro* and *in vivo*, performed the mouse studies and analysis of monocyte and TAM populations, the staining and scoring of human tumor samples and wrote the manuscript. SK helped with the mouse studies, all the statistical analyses, edited the figures and the manuscript. SS produced and purified the anti-CSF-1R antibody, stained tumor sections and helped with the mouse studies. AL performed the ELISAs and helped with the mouse studies. AJC helped with the mouse studies. MM performed and analyzed the secretion profiles of the different cancer cell lines. ZV provided the tumor tissue samples, scored G-CSF staining and performed statistical analyses. SJ and MD designed and discussed experiments, supervised progress, and edited the manuscript.

Disclosure of potential conflicts of interest

No potential conflicts of interest were disclosed.

Acknowledgments

We thank Jeannette Scholl, Heidi Baumberger, Silvia Crivelli, Sari Mäki, Mari Parsama and Linda Kauppinen for excellent technical assistance.

Funding

This work was supported by the ETH Zurich, Swiss Cancer League, Swiss National Science Foundation grant 310030B_147087, European Research Council grant LYVICAM and Leducq Foundation Transatlantic Network of Excellence grant Lymph Vessels in Obesity and Cardiovascular Disease (11CVD03) (to MD). MH was supported by the Sigrid Jusélius Foundation and the Instrumentarium Foundation.

References

- Boyle P. The globalisation of cancer. *Lancet* 2006; 368:629-30; PMID:16920452; [http://dx.doi.org/10.1016/S0140-6736\(06\)69225-8](http://dx.doi.org/10.1016/S0140-6736(06)69225-8)
- Boyle P. Triple-negative breast cancer: epidemiological considerations and recommendations. *Ann Oncol* 2012; 23 Suppl 6:v17-12; PMID:23012306; <http://dx.doi.org/10.1093/annonc/mds187>
- Crown J, O'Shaughnessy J, Gullo G. Emerging targeted therapies in triple-negative breast cancer. *Ann Oncol* 2012; 23 Suppl 6:v56-65; PMID:23012305; <http://dx.doi.org/10.1093/annonc/mds196>
- Mantovani A, Allavena P, Sica A, Balkwill F. Cancer-related inflammation. *Nature* 2008; 454:436-44; PMID:18650914; <http://dx.doi.org/10.1038/nature07205>
- Leek RD, Lewis CE, Whitehouse R, Greenall M, Clarke J, Harris AL. Association of macrophage infiltration with angiogenesis and prognosis in invasive breast carcinoma. *Cancer Res* 1996; 56:4625-9; PMID:8840975
- Mahmoud SM, Lee AH, Paish EC, Macmillan RD, Ellis IO, Green AR. Tumour-infiltrating macrophages and clinical outcome in breast cancer. *J Clin Pathol* 2012; 65:159-63; PMID:22049225; <http://dx.doi.org/10.1136/jclinpath-2011-200355>
- Mantovani A, Sica A. Macrophages, innate immunity and cancer: balance, tolerance, and diversity. *Curr Opin Immunol* 2010; 22:231-7; PMID:20144856; <http://dx.doi.org/10.1016/j.coi.2010.01.009>
- Mantovani A, Sozzani S, Locati M, Allavena P, Sica A. Macrophage polarization: tumor-associated macrophages as a paradigm for polarized M2 mononuclear phagocytes. *Trends Immunol* 2002; 23:549-55; PMID:12401408; [http://dx.doi.org/10.1016/S1471-4906\(02\)02302-5](http://dx.doi.org/10.1016/S1471-4906(02)02302-5)
- Stein M, Keshav S, Harris N, Gordon S. Interleukin 4 potently enhances murine macrophage mannose receptor activity: a marker of alternative immunologic macrophage activation. *J Exp Med* 1992; 176:287-92; PMID:1613462; <http://dx.doi.org/10.1084/jem.176.1.287>
- Pucci F, Venneri MA, Biziato D, Nonis A, Moi D, Sica A, Di Serio C, Naldini L, De Palma M. A distinguishing gene signature shared by tumor-infiltrating Tie2-expressing monocytes, blood "resident" monocytes, and embryonic macrophages suggests common functions and developmental relationships. *Blood* 2009; 114:901-14; PMID:19383967; <http://dx.doi.org/10.1182/blood-2009-01-200931>
- Sica A, Sacconi A, Bottazzi B, Polentarutti N, Vecchi A, van Damme J, Mantovani A. Autocrine production of IL-10 mediates defective IL-12 production and NF-kappa B activation in tumor-associated macrophages. *J Immunol* 2000; 164:762-7; PMID:10623821; <http://dx.doi.org/10.4049/jimmunol.164.2.762>
- Stockmann C, Doedens A, Weidemann A, Zhang N, Takeda N, Greenberg JI, Cheresch DA, Johnson RS. Deletion of vascular endothelial growth factor in myeloid cells accelerates tumorigenesis. *Nature* 2008; 456:814-8; PMID:18997773; <http://dx.doi.org/10.1038/nature07445>
- Lin EY, Nguyen AV, Russell RG, Pollard JW. Colony-stimulating factor 1 promotes progression of mammary tumors to malignancy. *J Exp Med* 2001; 193:727-40; PMID:11257139; <http://dx.doi.org/10.1084/jem.193.6.727>
- Aharinejad S, Paulus P, Sioud M, Hofmann M, Zins K, Schäfer R, Stanley ER, Abraham D. Colony-stimulating factor-1 blockade by antisense oligonucleotides and small interfering RNAs suppresses growth of human mammary tumor xenografts in mice. *Cancer Res* 2004; 64:5378-84; PMID:15289345; <http://dx.doi.org/10.1158/0008-5472.CAN-04-0961>
- Paulus P, Stanley ER, Schäfer R, Abraham D, Aharinejad S. Colony-stimulating factor-1 antibody reverses chemoresistance in human MCF-7 breast cancer xenografts. *Cancer Res* 2006; 66:4349-56; PMID:16618760; <http://dx.doi.org/10.1158/0008-5472.CAN-05-3523>
- Ryder M, Gild M, Hohl TM, Pamer E, Knauf J, Ghossein R, Joyce JA, Fagin JA. Genetic and pharmacological targeting of CSF-1/CSF-1R inhibits tumor-associated macrophages and impairs BRAF-induced thyroid cancer progression. *PLoS One* 2013; 8:e54302; PMID:23372702; <http://dx.doi.org/10.1371/journal.pone.0054302>
- Pyonteck SM, Akkari L, Schuhmacher AJ, Bowman RL, Sevenich L, Quail DF, Olson OC, Quick ML, Huse JT, Teijeiro V et al. CSF-1R inhibition alters macrophage polarization and blocks glioma progression. *Nat Med* 2013; 19:1264-72; PMID:24056773; <http://dx.doi.org/10.1038/nm.3337>
- Ries CH, Cannarile MA, Hoves S, Benz J, Wartha K, Runza V, Rey-Giraud F, Pradel LP, Feuerhake F, Klamann I et al. Targeting Tumor-Associated Macrophages with Anti-CSF-1R Antibody Reveals a Strategy for Cancer Therapy. *Cancer Cell*, 2014; 25(6):846-59; PMID: 24898549; <http://dx.doi.org/10.1016/j.ccr.2014.05.016>
- Görge I, Hartung T, Leist M, Niehörster M, Tiegs G, Uhlig S, Weitzel F, Wendel A. Granulocyte colony-stimulating factor treatment protects rodents against lipopolysaccharide-induced toxicity via suppression of systemic tumor necrosis factor-alpha. *J Immunol* 1992; 149:918-24; PMID:1378868
- Fraser AR, Cook G, Franklin IM, Templeton JG, Campbell M, Holyoake TL, Campbell JD. Immature monocytes from G-CSF-mobilized peripheral blood stem cell collections carry surface-bound IL-10 and have the potential to modulate alloreactivity. *J Leukoc Biol* 2006; 80:862-9; PMID:16895973; <http://dx.doi.org/10.1189/jlb.0605297>
- Boneberg EM, Hareng L, Gantner F, Wendel A, Hartung T. Human monocytes express functional receptors for granulocyte colony-stimulating factor that mediate suppression of monokines and interferon-gamma. *Blood* 2000; 95:270-6; PMID:10607712
- Klangsinsirikul P, Russell NH. Peripheral blood stem cell harvests from G-CSF-stimulated donors contain a skewed Th2 CD4 phenotype and a predominance of type 2 dendritic cells. *Exp Hematol* 2002; 30:495-501; PMID:12031657; [http://dx.doi.org/10.1016/S0301-472X\(02\)00785-3](http://dx.doi.org/10.1016/S0301-472X(02)00785-3)
- Hollmén M, Roudnicky F, Karaman S, Detmar M. Characterization of macrophage - cancer cell crosstalk in estrogen receptor positive and

- triple-negative breast cancer. *Sci Rep* 2015; 5:9188; PMID:25776849; <http://dx.doi.org/10.1038/srep09188>
24. Giricz O, Calvo V, Peterson EA, Abouzeid CM, Kenny PA. TACE-dependent TGF α shedding drives triple-negative breast cancer cell invasion. *Int J Cancer* 2013; 133:2587-95; PMID:23729230
 25. West NR, Murray JJ, Watson PH. Oncostatin-M promotes phenotypic changes associated with mesenchymal and stem cell-like differentiation in breast cancer. *Oncogene* 2014; 33:1485-94; PMID:23584474; <http://dx.doi.org/10.1038/onc.2013.105>
 26. Lehmann BD, Bauer JA, Chen X, Sanders ME, Chakravarthy AB, Shtyr Y, Pietenpol JA. Identification of human triple-negative breast cancer subtypes and preclinical models for selection of targeted therapies. *J Clin Invest* 2011; 121:2750-67; PMID:21633166; <http://dx.doi.org/10.1172/JCI45014>
 27. Phan VT, Wu X, Cheng JH, Sheng RX, Chung AS, Zhuang G, Tran C, Song Q, Kowanetz M, Sambrone A et al. Oncogenic RAS pathway activation promotes resistance to anti-VEGF therapy through G-CSF-induced neutrophil recruitment. *Proc Natl Acad Sci U S A* 2013; 110:6079-84; PMID:23530240; <http://dx.doi.org/10.1073/pnas.1303302110>
 28. Medrek C, Pontén F, Jirstrom K, Leandersson K. The presence of tumor associated macrophages in tumor stroma as a prognostic marker for breast cancer patients. *BMC Cancer* 2012; 12:306; PMID:22824040; <http://dx.doi.org/10.1186/1471-2407-12-306>
 29. Aslakson CJ, Miller FR. Selective events in the metastatic process defined by analysis of the sequential dissemination of subpopulations of a mouse mammary tumor. *Cancer Res* 1992; 52:1399-405; PMID:1540948
 30. Waight JD, Hu Q, Miller A, Liu S, Abrams SI. Tumor-derived G-CSF facilitates neoplastic growth through a granulocyte myeloid-derived suppressor cell-dependent mechanism. *PLoS One* 2011; 6:e27690; PMID:22110722; <http://dx.doi.org/10.1371/journal.pone.0027690>
 31. Mitsui T, Watanabe S, Taniguchi Y, Hanada S, Ebihara Y, Sato T, Heike T, Mitsuyama M, Nakahata T, Tsuji K. Impaired neutrophil maturation in truncated murine G-CSF receptor-transgenic mice. *Blood* 2003; 101:2990-5; PMID:12672695; <http://dx.doi.org/10.1182/blood.V101.8.2990>
 32. Kowanetz M, Wu X, Lee J, Tan M, Hagenbeek T, Qu X, Yu L, Ross J, Korsisaari N, Cao T et al. Granulocyte-colony stimulating factor promotes lung metastasis through mobilization of Ly6G+Ly6C+ granulocytes. *Proc Natl Acad Sci U S A* 2010; 107:21248-55; PMID:21081700; <http://dx.doi.org/10.1073/pnas.1015855107>
 33. Shojaei F, Wu X, Qu X, Kowanetz M, Yu L, Tan M, Meng YG, Ferrara N. G-CSF-initiated myeloid cell mobilization and angiogenesis mediate tumor refractoriness to anti-VEGF therapy in mouse models. *Proc Natl Acad Sci U S A* 2009; 106:6742-7; PMID:19346489; <http://dx.doi.org/10.1073/pnas.0902280106>
 34. Swierczak A, Cook AD, Lenzo JC, Restall CM, Doherty JP, Anderson RL, Hamilton JA. The promotion of breast cancer metastasis caused by inhibition of CSF-1R/CSF-1 signaling is blocked by targeting the G-CSF receptor. *Cancer Immunol Res* 2014; 2:765-76; PMID:25005824; <http://dx.doi.org/10.1158/2326-6066.CCR-13-0190>
 35. Rutella S, Zavala F, Danese S, Kared H, Leone G. Granulocyte colony-stimulating factor: a novel mediator of T cell tolerance. *J Immunol* 2005; 175:7085-91; PMID:16301609; <http://dx.doi.org/10.4049/jimmunol.175.11.7085>
 36. Bharadwaj U, Li M, Zhang R, Chen C, Yao Q. Elevated interleukin-6 and G-CSF in human pancreatic cancer cell conditioned medium suppress dendritic cell differentiation and activation. *Cancer Res* 2007; 67:5479-88; PMID:17545630; <http://dx.doi.org/10.1158/0008-5472.CAN-06-3963>
 37. Toyoda M, Chikamatsu K, Sakakura K, Fukuda Y, Takahashi K, Miyashita M, Shimamura K, Furuya N. A case of squamous cell carcinoma of the head and neck producing granulocyte-colony stimulating factor with marked leukocytosis. *Auris Nasus Larynx* 2007; 34:267-71; PMID:17097253; <http://dx.doi.org/10.1016/j.anl.2006.07.014>
 38. Ito N, Matsuda T, Kakehi Y, Takeuchi E, Takahashi T, Yoshida O. Bladder cancer producing granulocyte colony-stimulating factor. *N Engl J Med* 1990; 323:1709-10; PMID:1700300
 39. Obara T, Ito Y, Kodama T, Fujimoto Y, Mizoguchi H, Oshimi K, Takahashi M, Hirayama A. A case of gastric carcinoma associated with excessive granulocytosis. Production of a colony-stimulating factor by the tumor. *Cancer* 1985; 56:782-8; PMID:3874682; [http://dx.doi.org/10.1002/1097-0142\(19850815\)56:4%3c782::AID-CNCR2820560414%3e3.0.CO;2-5](http://dx.doi.org/10.1002/1097-0142(19850815)56:4%3c782::AID-CNCR2820560414%3e3.0.CO;2-5)
 40. Morris KT, Khan H, Ahmad A, Weston LL, Nofchissey RA, Pinchuk IV, Beswick EJ. G-CSF and G-CSFR are highly expressed in human gastric and colon cancers and promote carcinoma cell proliferation and migration. *Br J Cancer* 2014; 110:1211-20; PMID:24448357; <http://dx.doi.org/10.1038/bjc.2013.822>
 41. Nagata S, Tsuchiya M, Asano S, Yamamoto O, Hirata Y, Kubota N, Oheda M, Nomura H, Yamazaki T. The chromosomal gene structure and two mRNAs for human granulocyte colony-stimulating factor. *EMBO J* 1986; 5:575-81; PMID:2423327
 42. Stein J, Borzillo GV, Rettenmier CW. Direct stimulation of cells expressing receptors for macrophage colony-stimulating factor (CSF-1) by a plasma membrane-bound precursor of human CSF-1. *Blood* 1990; 76:1308-14; PMID:2145044
 43. Gluz O, Liedtke C, Gottschalk N, Pusztai L, Nitz U, Harbeck N. Triple-negative breast cancer—current status and future directions. *Ann Oncol* 2009; 20:1913-27; PMID:19901010; <http://dx.doi.org/10.1093/annonc/mdp492>
 44. Rimawi MF, Shetty PB, Weiss HL, Schiff R, Osborne CK, Chamness GC, Elledge RM. Epidermal growth factor receptor expression in breast cancer association with biologic phenotype and clinical outcomes. *Cancer* 2010; 116:1234-42; PMID:20082448; <http://dx.doi.org/10.1002/cncr.24816>
 45. Chung AS, Wu X, Zhuang G, Ngu H, Kasman I, Zhang J, Vernes JM, Jiang Z, Meng YG, Peale FV et al. An interleukin-17-mediated paracrine network promotes tumor resistance to anti-angiogenic therapy. *Nat Med* 2013; 19:1114-23; PMID:23913124; <http://dx.doi.org/10.1038/nm.3291>
 46. Granot Z, Henke E, Comen EA, King TA, Norton L, Benezra R. Tumor entrained neutrophils inhibit seeding in the premetastatic lung. *Cancer Cell* 2011; 20:300-14; PMID:21907922; <http://dx.doi.org/10.1016/j.ccr.2011.08.012>
 47. Asano K, Nabeyama A, Miyake Y, Qiu CH, Kurita A, Tomura M, Kanagawa O, Fujii S, Tanaka M. CD169-positive macrophages dominate antitumor immunity by crosspresenting dead cell-associated antigens. *Immunity* 2011; 34:85-95; PMID:21194983; <http://dx.doi.org/10.1016/j.immuni.2010.12.011>
 48. Ohnishi K, Komohara Y, Saito Y, Miyamoto Y, Watanabe M, Baba H, Takeya M. CD169-positive macrophages in regional lymph nodes are associated with a favorable prognosis in patients with colorectal carcinoma. *Cancer Sci* 2013; 104:1237-44; PMID:23734742; <http://dx.doi.org/10.1111/cas.12212>
 49. Saito Y, Ohnishi K, Miyashita A, Nakahara S, Fujiwara Y, Horlad H, Motoshima T, Fukushima S, Jinnin M, Ihn H et al. Prognostic Significance of CD169+ Lymph Node Sinus Macrophages in Patients with Malignant Melanoma. *Cancer Immunol Res* 2015; Dec; 3(12):1356-63; PMID:26297710
 50. Neve RM, Chin K, Fridlyand J, Yeh J, Baehner FL, Fevr T, Clark L, Bayani N, Coppe JP, Tong F et al. A collection of breast cancer cell lines for the study of functionally distinct cancer subtypes. *Cancer Cell* 2006; 10:515-27; PMID:17157791; <http://dx.doi.org/10.1016/j.ccr.2006.10.008>
 51. Theurillat JP, Ingold F, Frei C, Zippelius A, Varga Z, Seifert B, Chen YT, Jäger D, Knuth A, Moch H. NY-ESO-1 protein expression in primary breast carcinoma and metastases: correlation with CD8+ T-cell and CD79a+ plasmacytic/B-cell infiltration. *Int J Cancer* 2007; 120:2411-7; PMID:17294444; <http://dx.doi.org/10.1002/ijc.22376>
 52. Movahedi K, Laoui D, Gysemans C, Baeten M, Stangé G, Van den Bossche J, Mack M, Pipeleers D, In't Veld P, De Baetselier P et al. Different tumor microenvironments contain functionally distinct subsets of macrophages derived from Ly6C(high) monocytes. *Cancer Res* 2010; 70:5728-39; PMID:20570887; <http://dx.doi.org/10.1158/0008-5472.CAN-09-4672>